Published in final edited form as:
Q J Nucl Med Mol Imaging. 2010 June ; 54(3): 259–280.

Multimodality imaging of hypoxia in preclinical settings

Ralph P. Mason, **Dawen Zhao**, **Jesús Pacheco-Torres**, **Weina Cui**, **Vikram D. Kodibagkar**, **Praveen K. Gulaka**, **Guiyang Hao**, **Philip Thorpe**, **Eric W. Hahn**, and **Peter Peschke**[1]
Department of Radiology, U.T. Southwestern Medical Center, Dallas, TX

[1] DKFZ, German Cancer Research Center, Heidelberg

Abstract

Hypoxia has long been recognized to influence solid tumor response to therapy. Increasingly, hypoxia has also been implicated in tumor aggressiveness, including growth, development and metastatic potential. Thus, there is a fundamental, as well as a clinical interest, in assessing *in situ* tumor hypoxia. This review will examine diverse approaches focusing on the pre-clinical setting, particularly, in rodents. The strategies are inevitably a compromise in terms of sensitivity, precision, temporal and spatial resolution, as well as cost, feasibility, ease and robustness of implementation. We will review capabilities of multiple modalities and examine what makes them particularly suitable for investigating specific aspects of tumor pathophysiology. Current approaches range from nuclear imaging to magnetic resonance and optical, with varying degrees of invasiveness and ability to examine spatial heterogeneity, as well as dynamic response to interventions. Ideally, measurements would be non-invasive, exploiting endogenous reporters to reveal quantitatively local oxygen tension dynamics. A primary focus of this review is magnetic resonance imaging (MRI) based techniques, such as ^{19}F MRI oximetry, which reveals not only hypoxia *in vivo*, but more significantly, spatial distribution of pO_2 quantitatively, with a precision relevant to radiobiology. It should be noted that pre-clinical methods may have very different criteria for acceptance, as compared with potential investigations for prognostic radiology or predictive biomarkers suitable for use in patients.

Keywords

hypoxia; magnetic resonance imaging; hexafluorobenzene; oxygen; tumor; fluorine; BOLD

1. Introduction

Hypoxia and tissue oxygenation comprise a vast field of study relevant to diverse diseases. This review focuses on its relevance to solid *in situ* tumor development, progression, and primarily response to therapy. Studies range from molecular biology to therapeutic oncology with a common thread of imaging based on developments in reporter molecules, physics, engineering and data processing.

Ever since the classic studies of Gray *et al.* fifty years ago (1), it has been appreciated that hypoxia can influence the efficacy of radiotherapy on tumors. There have been many attempts to modulate tumor hypoxia in order to enhance radiotherapy, but translation to the clinic has shown marginal efficacy (2). The meta analysis by Overgaard *et al.* (3) of some 10,000 patients indicated a clinical benefit for manipulating tumor hypoxia. However, the

RALPH P. MASON, Ph.D., CSci, CChem, Professor of Radiology, The University of Texas Southwestern Medical Center, 5323 Harry Hines Boulevard, Dallas, Texas 75390-9058, Tel: 214-648-8926, FAX: 214-648-2991, Ralph.Mason@UTSouthwestern.edu.

overall conclusion was that there was a pressing need to identify those tumors (*viz*. patients), who would actually benefit.

In terms of hypoxia in human tumors, we perceive three needs: 1) to develop an effective method of detecting hypoxia non-invasively in tumors of patients prior to therapy; 2) to assess the ability to modulate tumor hypoxia to overcome resistance to therapy; 3) to exploit hypoxia using specific individualized patient therapies, which are effective on hypoxic cells. We believe we are at a historic juncture, where we not only have technologies for identifying hypoxia, but more importantly methods of tailoring therapy successfully to accommodate or exploit the killing of hypoxic cells.

One aspect of pre-clinical research is simply to develop methods satisfying the clinical requirements. However, for pre-clinical applications themselves, we perceive slightly modified needs, firstly: effective methods of assaying tumor hypoxia, and secondly: well-characterized animal models with tumors exhibiting well-defined differential levels of hypoxia and responses to interventions. Criteria for useful methods are also somewhat different, *e.g.*, imaging methods may rely on reporter molecules, which are efficient and ethical for use in small animal studies, but do not have, and might not meet, requirements for patients (notably, IND). The requirements are not necessarily less stringent.

Early work on effects of hypoxia examined cells *in vitro*, where ambient oxygen concentrations are readily controlled. *In vivo*, hypoxia may be achieved by clamping the blood supply to a tumor (4), but other levels of oxygenation reflect the interplay of supply and consumption (5). Given the importance of hypoxia many methods have been developed for probing tumor oxygenation including hypoxia reporter agents, polarographic electrodes, fiber optic probes, NIR spectroscopy, and various NMR techniques, but most are either highly invasive, lack spatial resolution or lack the ability to dynamically and quantitatively sample the response to intervention (2,6–8) (Table 1).

2.0 Hypoxia

The concept of hypoxia may be debated, but presumably indicates oxygen insufficiency. Anoxia is presumed to be complete absence of molecular oxygen and this may be achieved in model systems and cell cultures. Indeed, cell culture incubators are available to exclude and eliminate oxygen, as required for the culture of facultative anaerobes. More commonly, cell cultures are saturated with a gaseous atmosphere of specific oxygen concentration and cells are adapted to growth under low pO_2 saturation.

In the heart and brain, hypoxia may be attributed to ischemia, where the delivery of oxygen is insufficient to maintain normal function. Ischemia may be total, or partial, and it may manifest itself as chest pain, angina or even be silent for many years, while chronic damage is established. Hypoxia may occur due to local lack of vascular flow or insufficient hemoglobin saturation. An acute myocardial infarct will result in rapid oxygen depletion and loss of mechanical function. We have shown, as expected, using ^{19}F NMR of perfluorocarbons sequestered in the myocardium that hypoxiation is much more rapid in a beating heart than an arrested heart, and indeed, the rate of loss of developed pressure is directly proportional to decrease in pO_2 (9).

However, in tumors, a definition of hypoxia may be far more complex, since the tissue is aberrant with no particular normal function, yet well documented ability to adapt to stress. Hypoxia has been shown to stimulate mutations, and hypoxic stress appears to stimulate angiogenesis and metastasis, particularly, as a result of intermittent bouts of hypoxic stress (10–12). Tumor cells may survive in quite hypoxic conditions, but for a solid tumor to grow beyond a few hundred microns in diameter, an angiogenic switch is required to generate new

blood vessels for the delivery of nutrients and oxygen (13). In hypoxic conditions, tumor cells release angiogenic factors stimulating blood vessel sprouting and a new vascular network. Figure 1 shows typical chaotic vascular extent, and thus tumors are expected to be hypoxic. In terms of Figure 1d, it is noteworthy that externalization of phosphatidylserine (PS) to the luminal surface of the vascular endothelium is stimulated by stress including hypoxia (14). Consequently, phosphatidylserine is a marker of tumor vasculature and a potential target for anti-cancer drugs. The exposed PS is one of the most specific markers of tumor vasculature yet discovered and provides an excellent marker for imaging with radionuclide-bavituximab conjugates (15).

The expression of many proteins is influenced by hypoxia (16,17) and hypoxia sensitive promoter regions have been developed to generate hypoxia responsive reporter genes. A specific promoter regulating a reporter gene, such as luciferase or fluorescent protein (*e.g.*, eGFP), can selectively turn on expression under hypoxic conditions. Often, multiple promoter copies are exploited to avoid expression leakage and an oxygen degradation domain may be incorporated (18). This approach requires transfection of cells and reporter proteins may remain for several hours after amelioration of hypoxia, preventing acute dynamic studies. This approach is particularly suitable for observing onset of chronic hypoxia (19). In small animals, optical imaging has the advantages of being cheap, generally simple to implement on commercial instruments, and allows high throughput. Fluorescent proteins may be detected non-invasively, although depth of light penetration limits studies to small animals or surface tissues. Luciferase does require administration of luciferin substrate.

It has long been appreciated that hypoxic tumor cells are more resistant to radiotherapy (1). Indeed, a threefold increase in radio-resistance may occur when cells are irradiated under hypoxic conditions compared with $pO_2 > 15$ torr for a given single radiation dose. However, recent modeling has indicated that the proportion of cells in the range 0 – 20 torr may be most significant in terms of surviving a course of fractionated radiotherapy (20). The clinical significance of hypoxia for radiotherapy was recently illustrated by modeling the radiation response of a heterogeneous cell population. Based on an oxygen enhancement ratio of 3.0, Fowler *et al.* (21) demonstrated that while a fractionated dose of 70–80 Gy would lead to reduction in cell survival from 1 to 10^{-12} for a well-oxygenated tumor, a similar reduction in survival would require a dose exceeding 200 Gy for a tumor containing 20% hypoxic cells. In the clinical setting, we expect hypoxia to be even more important for high dose fractionation protocols, which are gaining feasibility based on precise treatment plans and effective targeting. Timmerman *et al.* (22) recently reported results of The Radiation Therapy Oncology Group (RTOG) protocol RTOG 0236 Phase II trial utilizing stereotactic body radiation therapy (SBRT) with ablative prescription dose to treat early-stage medically inoperable non–small-cell lung cancer (NSCLC) patients. Using three doses of 20 Gy in less than two weeks, the estimated 2-year survival exceeded 90%, which is a remarkable improvement over traditional therapy. When few doses are applied, the hypoxic fraction is expected to have much greater impact on radioresistance, since there is no opportunity for the progressive reoxygenation and repopulation attributed to long-term fractionated irradiation and thus methods of assessing hypoxia are increasingly relevant.

When hypoxia is identified several options arise: i) “dose-painting”, booster regimens and IMRT have been proposed and are being tested (23–26), ii) administering adjuvant hypoxic cell selective cytotoxins: clinical trials with tirapazamine were halted, but new, potentially, more effective drugs are being developed, *e.g.*, AQ4N and TH302 (27,28); iii) a simpler intervention would be breathing hyperoxic gas to ameliorate the hypoxia. Indeed, many clinical trials have explored oxygen, carbogen or hyperbaric gas breathing, but with limited success, likely due to the inability to identify those patients with hypoxic tumors, who would

benefit. By analogy, assaying HER2/neu status is vital to the effective use of Herceptin (Trastuzumab) to treat breast cancer patients. Thus, a crucial concern is identifying those patients, who may need the adjuvant intervention and benefit and there is an urgent need to develop methods of indentifying potentially resistant hypoxic tumors and implementing adjuvant interventions. We note the report from Nijmegen (29), which showed that patients with large head and neck hypoxic tumors (identified using pimonidazole in biopsies) could be brought into the realm of effective response by applying the ARCON protocol (Accelerated Radiation therapy with Carbogen and Nicotinamide).

2.1 Radionuclide imaging of hypoxia: PET, SPECT and γ-scintigraphy

Given the importance of hypoxia diverse classes of reporter molecules have been developed to reveal hypoxia, *e.g*., pimonidazole (29,30), EF5 (31,32), CCI-103F (33), Cu-ATSM (34), galactopyranoside IAZA (35). Many reporters are based on the structure of misonidazole, which had been explored extensively as a radiation sensitizer. Unacceptable toxicity (neuropathy) halted clinical applications, but it was realized that reporter molecules could be used at much lower concentrations, *e.g*., 15 μg as opposed to 10 g per patient (17) allowing effective application. Indeed, beyond pre-clinical applications EF5, FAZA, Cu-ATSM and F-MISO are being evaluated in ongoing clinical trials (http://clinicaltrials.gov/).

Following *IV* infusion, the agents diffuse into tissues, where they are reduced forming highly reactive intermediates. In the presence of oxygen, they are reoxidized and ultimately clear from the body. However, in the absence of molecular oxygen, further reductions occur yielding radical anions and reactive alkylating amine derivatives, which are trapped in the cell (17). In biopsies, EF5 and pimonidazole are both routinely used in conjunction with fluorescent immunohistochemical analysis providing microscopic indications of local hypoxia (*e.g*., Fig. 1c shows hypoxia in a rat breast tumor distant from the well perfused regions) (36). EF5, pimonidazole, and Cu-ATSM are currently being tested in clinical trials and correlations have been reported relating uptake to clinical outcome (29,32,37). Over the past 20 years, many variant reporter molecules have been proposed focusing on modifying lipophilicity, reduction potential and reactivity. MRI has been applied to several fluoronitroimidazole derivatives including EF5 and SR-4554 (38,39).

Incorporation of radionuclides has facilitated non-invasive investigations using PET, SPECT or γ-scintigraphy, as reviewed extensively by others recently (8,17,40–42). The most widely used reporter has been fluoromisonidazole (F-MISO), which has been tested extensively in animals (Figure 2) and is being evaluated in clinical trials. F-18 has a relatively short half-life (110 mins), but an efficient synthesis was developed based on ^{18}F-fluoride and a pure racemic mixture suitable for injection into patients can be produced in 35 minutes with a specific activity of 250 GBq/μmol (17). Thus, a typical patient dose of 260 MBq requires only 0.2 μg. Patients are normally imaged 1.5 hours after administration.

Early autographic studies based on tritiated F-MISO showed effective penetration into cultured cell spheroids with greatest concentration being at the interface of viable cells and the necrotic center. Under anoxic conditions, binding was found to be 25-fold greater than in normoxic conditions, where binding dropped to 40% at 4 mmHg (torr). *In vivo*, there is concern that distribution and uptake may be influenced by relative blood flow, which is likely to be particularly low in hypoxic regions. Correlative studies with the blood flow indicator ^{14}C-iodoantipyrine showed no correlation between flow and F-MISO binding (17). Krohn *et al.* (2) state that a tumor to background ratio less than unity is an indication of normoxic tissues, while values greater than 1.2 infer hypoxia. However, slow washout is a concern and alternative fluorinated derivatives have been evaluated, particularly exploring differential lipophilicity based on degree of fluorination (Table 2) (17). FAZA showed much

faster clearance from the blood of mice and while tumor uptake was less, the tumor to blood was significantly greater than for F-MISO (43).

Alternate agents use iodoazogalactosides or copper lactams and each is undergoing clinical trials (Table 2). I-124 allows PET and the longer half-life allows imaging after 24 to 48 hrs when background has cleared. Several studies have shown efficacy of this approach, but the signal to noise appears inferior to F-MISO (Fig. 2) (44). Iodine labeling has the added advantage of allowing several isotopes for different applications including PET (^{124}I), SPECT ($^{123, 125}$I), γ-scintigraphy (^{125}I) and radioimmunotherapy (^{131}I), although instability and dehalogenation can be problematical. Copper based agents are attractive, since they also allow multiple isotopes with longer half lives (^{60}Cu $t_{½}$ = 23 mins, 93% $\beta^{+;}$ ^{61}Cu $t_{½}$ = 3.3 hrs, 61% $\beta^{+;}$ ^{62}Cu $t_{½}$ = 9.7 mins; ^{64}Cu $t_{½}$ = 12.7 hrs, 17.4% β^{+} for PET; and ^{67}Cu $t_{½}$ = 61 hrs for therapy) (45). Cu-ATSM shows specificity for hypoxic tissues and has shown correlation with clinical outcome for lung and cervical cancer patients (34,37). However, uptake and retention appears to be inconsistent in some cells and may be influenced by protein expression related to multi drug resistance (46,47). Early PET studies had used ^{60}Cu-PTSM, but recently Lewis *et al.* (48) showed that ^{64}Cu-PTSM was equally applicable in patients with cervical cancer and indeed the image quality was reported to be better (Figure 3). However, differences in image quality may be attributed to some variation in data acquisition including 2D versus 3D to avoid contamination from daughter nuclides. Copper-64 is increasingly available from commercial sources to generate such labels, *e.g.*, MDSNordion (Canada), ACOM(Italy), Trace Life Sciences (United States), IBA Molecular (United States and Europe), and IsoTrace (United States). The longer half-life promises a more convenient radiopharmaceutical. Beyond nuclides of iodine and copper, one can envision an arsenic nitroimidazole, where the isotopes $^{72, 74 \text{ and } 77}$As provide diverse opportunities for PET and radiotherapy (15,49).

^{18}F-misonidazole shows considerable promise in clinical trials, though the rapid decay of F-18 is inconvenient. There have been attempts to correlate the more standard fluorodeoxyglucose (FDG) uptake with hypoxia, but correlations are often poor (50).

Nuclear medicine approaches are costly and less suitable for repeat investigations. Generally, only a single time point is investigated and the measurement is thought to reflect chronic hypoxia, rather than acute hypoxia. For PET, each reporter provides identical signal and thus repeat doses or tandem reporters cannot be readily differentiated except perhaps based on differential decay rates of separate isotopes. Dynamic variations in hypoxia have been assessed, based on biopsy specimens, by applying pairs of hypoxia reporters in a pulse chase fashion with respect to an intervention, as shown by Ljungkvist *et al.* (33). NMR spectroscopy of ^{19}F-misonidazoles potentially allows greater versatility, since multiple different reporters could be detected simultaneously based on separate resolved chemical shifts, but it must be noted that NMR requires much higher concentration of reporter molecule (9). An alternative approach is to exploit an MRI reporter, which has physical characteristics influenced by oxygen and detectable by relaxometry as described in the next sections (6).

3.0 Tumor Oximetry: *In vivo*

While hypoxia may have a somewhat arbitrary definition, oximetry provides quantitative assessment of pO_2. In turn pO_2 can define hypoxic thresholds such as fraction of tumor less than 10 torr (HF_{10}) or HF_5 < 5 torr. It should be noted that various scales are used to report pO_2 [760 torr = 1 atm = 101 kPa], and that pO_2 is related to the concentration of dissolved oxygen [O_2]. It is important to consider the location of the pO_2 measurement, since there are steep gradients from vasculature to interstitium, cytosol and mitochondrion as emphasized

by Swartz (51). Ultimately, a parameter must correlate with therapeutic outcome, be reproducible and simple to implement and interpret.

To date, the most extensive evidence for hypoxia in experimental solid tumors is provided by polarographic needle oxygen electrodes. Robust fine needle polarographic electrodes opened the possibility of measuring pO_2 in tumors *in situ in vivo* to define local pO_2 under baseline conditions or with respect to interventions. Cater and Silver (52) showed the ability to monitor pO_2 at individual locations in patients' tumors with respect to breathing oxygen. The Eppendorf Histograph has provided the most convincing evidence for hypoxia in human tumors (53–55) and has been considered a "gold standard", but it is highly invasive. Following extensive studies in animals, the Histograph was used in the clinical setting and has unequivocally revealed hypoxia in many tumor types, *e.g*., head and neck, cervix, breast, and prostate and even intraoperative deflated lung (2). Moreover, pO_2 distributions have been found to have prognostic value. Disease free survival is significantly worse for patients with hypoxic tumors and applications to cervical cancer have shown correlation between tumor hypoxia and response to irradiation (56). In addition hypoxic tumors have been shown to have poorer response with surgical resection and this is considered to reflect a more aggressive hypoxic phenotype (10,56,57). By stepping the electrode through a tumor pO_2 distributions are determined providing a quasi map, though normally presented just in terms of a histogram. Chapman *et al*. (58) determined that as many as 100 individual locations were required to reproducibly/reliably represent tumor oxygenation. The Eppendorf reveals a pO_2 distribution, which is invariably skewed towards hypoxia. The distribution reported by the histogram reveals heterogeneity, but requires effective data reduction to be useful as a prognostic or predictive biomarker. Variously, mean, median or hypoxic fraction have been reported to correlate with therapeutic response. Hypoxic fraction may be described as HF_{10}, HF_5 or $HF_{2.5}$ and may be quoted as a ratio to normal adjoining tissue. The Eppendorf Histograph is not well suited for dynamic measurement of pO_2 with respect to intervention, though repeated measurement in patients with cervical cancer showed that oxygen or carbogen increased tumor oxygenation (59,60). The Histograph requires tissue access and is impractical in many tumors.

Fiber optic probes can also measure pO_2 directly and are typically finer and do not consume oxygen during measurement. Typically, two or four locations are sampled simultaneously and these optical probes facilitate observation of dynamic changes in pO_2 in response to interventions (61,62). Fiber optic probes are generally most sensitive to low pO_2 providing little sensitivity above 100 torr.

ESR has been exploited effectively, using both vascular probes and injected implanted particulates (63–65). Most importantly, ESR of implanted carbon chars revealed reoxygenation, in tumors and a correlation with response to irradiation based on measurements at a single location (66). Gallez, *et al*., investigated many drugs and interventions using ESR and found that several drugs will enhance tumor oxygenation (67).

Materials may be monitored for weeks to months with no apparent deleterious side effects in normal tissue. However, ESR is not readily available for pre-clinical applications and it is essentially impossible in patients due to lack of instrumentation.

3.1 Oximetry Imaging Methods

Given the importance of tumor oxygenation, many diverse methods have been developed and multiple reviews compare and contrast efficiency of imaging approaches. As such, the reader is directed to these articles for historical perspective. In 2004, the NCI sponsored a workshop on hypoxia imaging technologies as summarized in a comprehensive review by Arbeit, *et al*. (2) featuring contributions from many of the leaders in the field. Imaging

approaches, together with needs for the measurements, are extensively described. Other recent reviews have focused on nuclear imaging approaches (8,17), optical methods (68), ESR (51,69) and MRI (6,70). Others have focused on the molecular biology and relevance to therapy and clinical trials (71,72). In Table 1, we summarize virtues and capabilities of popular methods. In the present review, we will focus on the latest innovations and our own experience with MRI.

In choosing a method, it is crucial to match the capabilities to the problem being addressed. Thus, predicting the efficacy of a hypoxic cell selective cytotoxin may well be ideal using a nitroimidazole reporter, which could exploit optical imaging, MRI or PET (73).

3.2 ^{19}F MRI

Most MRI oximetry exploits perfluorocarbons (PFCs), where the spin lattice relaxation rate ($R_1=1/T_1$) is exquisitely sensitive to pO_2 and obeys a linear relationship ($R_1= a + b\ pO_2$) at any given magnetic field and temperature. Historically, PFC emulsion blood substitutes were administered systemically (74). Following iv administration, they exhibit prolonged vascular circulation and can provide measurements of vascular pO_2 for several hours, though measurements are potentially susceptible to flow artifacts. Ultimately, PFCs become sequestered in tissue, primarily in the reticuloendothelial system (RES, liver, spleen and bone marrow) allowing pO_2 measurements (74). Small amounts are found in myocardium and tumor and have been exploited for oximetry. The early PFC emulsions (Fluosol^{TM}; Oxypherol^{TM} (perfluorotributylamine); Oxygent^{TM} (perfluorooctylbromide); Therox^{TM} (F44E)) had multiple resonances and the requirement for chemical shift selective imaging often caused signal loss. However, each signal showed unique sensitivity to pO_2 and temperature and this phenomenon could be exploited to determine both parameters simultaneously (75). Systemic administration had the great advantage of being non-invasive, but most of the small fraction of PFC, which became sequestered in the tumor was found in well perfused tumor regions biasing measurements (76).

Symmetrical PFCs may have a single ^{19}F resonance offering better signal to noise ratio. Fifteen-crown-five-ether has been used as an emulsion to probe liver and tumor pO_2 (77). Hexafluorobenzene (HFB) provides an alternative, which is more readily commercially available, more sensitive to changes in pO_2 and less sensitive to changes in temperature (6). Hexafluorobenzene has an extremely high vapor pressure bringing potential benefits or problems. It does not form stable biocompatible emulsions and requires direct injection into tissue. It also clears rapidly so that pO_2 measurements are generally only possible on the day of administration. Direct injection into a tissue has the distinct advantage that any region of interest may be interrogated immediately without needing to wait for vascular clearance. Moreover, there are no concerns about potential toxicity related to long-term retention. Hexafluorobenzene exhibits an extremely broad range of T_1 from 0.7 s to 13 s at 4.7 Tesla, so that imaging may be slow. Since signal to noise ratio (SNR) influences the precision of pO_2 measurements, the benefits of HFB may be less than anticipated (78). The potential long acquisition times required to assess long T_1s were overcome by applying echo planar imaging (EPI). We routinely achieve pO_2 maps with 50 to 150 individual locations simultaneously in 6½ minutes in rat tumors with a precision of 1 to 3 torr in hypoxic regions following administration of 50 μl HFB. We have used the so-called FREDOM approach (Fluorocarbon Relaxometry using Echo planar imaging for Dynamic Oxygen Mapping) to examine multiple tumor types implanted in rats and mice including breast, lung and prostate. Representative images and data are shown in Figures 4–7 and Table 3. As expected, median pO_2 and hypoxic faction observed in rat tumors were inversely related (Figure 5).

We have applied this approach to multiple studies and have demonstrated measurements commensurate with more traditional techniques such as polarographic electrodes (including

the Eppendorf Histograph) (79,80), optical fiber probes (62), immunohistochemistry (81), and near-infrared spectroscopy (82), in terms of baseline pO_2 and response to interventions.

The greatest strength of ^{19}F MRI is the ability to make sequential measurements over a period of hours with respect to interventions. Maps of pO_2 allow individual tumor regions to be monitored or cluster analysis reveals differential behavior for regions showing shared baseline characteristics. In some cases, the baseline measurement is indicative of response to intervention such as breathing hyperoxic gas (Figure 5b). For most tumors, we find that initially well oxygenated tumor regions show a particularly large response to hyperoxic gas breathing (83). In virtually every mouse and rat tumor system examined to date, we found progressive hypoxiation with increased size (Table 3 + Figure 6) (62, 81, 84). Small tumors are generally well oxygenated with small hypoxic fractions, but somewhere between 1 and 3 cm^3 a catastrophic decline occurs in oxygen tension (62, 81, 84).

It is well documented that hypoxia leads to radiation resistance. During a course of conventional fractionated radiotherapy, progressive re-oxygenation is reported to occur. However, for a single dose or limited sequential doses, hypoxic fraction may be far more important. We have shown that irradiation (single dose 30 Gy) of large hypoxic Dunning prostate R3327-HI tumors caused limited tumor growth delay (Figure 6). However, this tumor type shows a pronounced oxygenation accompanying hyperoxic gas breathing, essentially eliminating the hypoxic fraction (HF_{10} < 20%; Table 3). With oxygen breathing there was a significant tumor growth delay accompanying the same single dose of irradiation (85). By contrast, in small HI tumors, where the HF_{10} <20 torr for air breathing, there was a significant tumor growth delay accompanying irradiation and no additional benefit was seen for breathing oxygen (Figure 6). We note that large AT1 tumors, which exhibit a high hypoxic fraction that resists modulation also show minimal benefit from breathing oxygen (86). Thus, measurements of baseline pO_2 may be indicative of radiation response and assessment of the ability to manipulate tumor oxygenation using an intervention may be relevant to predicting such adjuvant interventions for enhancing radiation. Noting that some tumors resist hyperoxic gas breathing, it is tempting to apply hyperbaric oxygen and indeed using fiber optic probes, we showed that hypoxic regions of tumors, which resisted modulation by 100% normobaric oxygen, did respond to hyperbaric oxygen (87). We have previously shown that vasoactive drugs, such as hydralazine caused reduced tumor oxygenation (88). As expected, the vascular disrupting agent Combretastatin A4P caused rapid hypoxiation (89) and preliminary data show that this strongly influences the efficacy of combined radiation therapy. Meanwhile, the vascular targeting agent, bavituximab, has a minimal acute effect on pO_2 over a period of two hours (Figure 7).

3.3 ^{1}H MRI

For small animal studies, quantitative ^{19}F MRI oximetry of hexafluorobenzene (HFB) is very effective. There is no background signal and single resonance provides very high sensitivity to pO_2. However, we have been exploring proton MRI alternatives with view to greater translatability to the clinical setting. Noting the requisite properties of the ^{19}F perfluorocarbon reporters (hydrophobic, liquid, single resonance, unreactive, high gas solubility), we sought analogous proton agents and identified hexamethyldisiloxane (HMDSO) (90). Detection does require fat and water suppression, but this is routinely achieved for imaging metabolites such as N-acetyl aspartate, lactate, choline and citrate in brain or prostate of patients. Thus, proton magnetic resonance spectroscopy (90) or magnetic resonance imaging (91) may be used analogously to FREDOM (6) and we have initiated investigations using HMDSO (*e.g.*, PISTOL: Proton Imaging of Siloxanes to map Tissue Oxygenation Levels). We show an example of the detection of hypoxiation following administration of the vascular disrupting agent Combretastatin (CA4P) to a prostate tumor bearing rat in Figure 8 and this closely matches previous ^{19}F MRI results (89).

4.0 Endogenous reporters

Many reporter molecules are routinely exploited with diverse imaging modalities to measure tumor hypoxia or pO_2. Ideally, oxygenation could be related to endogenous characteristics. Since many biochemical pathways are under oxygen regulation, they can provide an elegant window on hypoxia, *e.g*., induction of HIF-1 and Glut-1 together with secondary responses, such as increased production of VEGF, NIP3 and tumor associated macrophage activity. However, assessment of expression requires biopsy. Additionally, the optical absorption spectra of oxy- and deoxyhemoglobin are quite different allowing interrogation of vascular oxygenation by spectroscopy and imaging though spatial resolution is generally quite poor (68,82). Deoxyhemoglobin is also paramagnetic and forms the basis of BOLD MRI.

4.1 BOLD (blood oxygen level dependent) contrast ^{1}H MRI

BOLD contrast depends on deoxyhemoglobin, which is paramagnetic. Deoxygenated red blood cells generate local magnetic field gradients causing signal dephasing, which appears as T_2* relaxation and can be detected as signal loss in T_2*-weighted images. The magnitude of the effect depends on hematocrit, vascular volume, and concentration of deoxyhemoglobin. Images may further be influenced by flow effects leading to the concept of FLOOD (FLow and Oxygen Level Dependant) (92). The BOLD effect is widely exploited in studies of brain activation, where stimuli generate regional changes in blood flow, altering deoxyhemoglobin concentration and generating contrast, which is the foundation of fMRI (93). In blood, a direct relationship is found between the T_2* and pO_2 based on the sigmoidal O_2 binding curve of hemoglobin. For large blood vessels T_2* may be used to measure vascular oxygenation, and hence pO_2, directly (94) and a recent development in the brain is sometimes referred to as qBOLD (95).

Interpretation of BOLD in tumors is more complex due to the bed of tortuous small capillaries, such that voxels include both blood vessels and surrounding tissue. Several groups have examined the effect and its relationship to tumor oxygenation, notably Howe, Robinson and Griffiths at St George's, London (92,96,97). A direct correlation between pO_2 and the BOLD signal changes has been found in several studies. Al Hallaq *et al*. (98) reported a strong linear correlation between change in pO_2 measured by electrode and change in the signal line widths (essentially T_2*). Elas *et al.* and Dunn *et al.* compared EPR (electron paramagnetic resonance) estimates of oxygenation and BOLD response and each found consistent data (65,99). We recently showed a strong correlation between changes in T_2*-weighted signal and pO_2 based on ^{19}F MR oximetry (100). Perhaps most significantly, we found that a large BOLD response (>2% ΔSI) to hyperoxic gas challenge (carbogen) corresponded with essential elimination of hypoxic fraction in rat breast tumors. Meanwhile, a small BOLD response generally indicated larger residual hypoxic fraction resistant to manipulation. Baudelet and Gallez reviewed BOLD investigations of tumors thoroughly (101) and also reported correlation of BOLD signal changes versus fiber optic oxygen tension measurements and oxygen challenge (102). The results indicated that there was always a positive correlation, but that a 10% change in relative signal intensity in the BOLD experiment could correspond to an increase in $pO_2 < 25$ torr or > 100 torr. We contend that either change would be radiobiologically pertinent, because once pO_2 exceeds 10 torr there is relatively little further oxygen enhancement achieved by increased levels of oxygen.

Currently, Padhani *et al.* are pursuing the use of BOLD to investigate tumors at various sites in patients with an emphasis on prostate cancer (103–105). Their primary method differs somewhat from our approach in that they assess baseline R_2* and relate it to inherent hypoxia rather than evaluating hypoxia based on the response to an oxygen breathing challenge. Rodrigues *et al*., showed that R_2* itself was indicative of hypoxia and correlated with response to radiation in tumors (106).

We note the BOLD response reflects vascular oxygenation, which may be disconnected from tissue pO_2. While increased oxygen delivery is expected to elevate local pO_2, the additional oxygen could be consumed, as noted by Gullino and Vaupel in studies of perfused tumors (107,108). Thus, we believe it is imperative to also include an assessment of tissue oxygenation (pO_2).

4.2 TOLD (Tissue oxygen level dependant) contrast ^{1}H MRI

Molecular oxygen (O_2) is paramagnetic and hence [O_2] influences tissue water spin-lattice relaxation (R_1). Recently, Matsumoto *et aI.* (109) demonstrated T_1 sensitive signal response in tumors to breathing hyperbaric oxygen, which reflects changes in tissue pO_2. Others have explored normal tissue response to hyperoxic gas breathing, notably Edelman *et al.* (110) and recently O'Connor *et al.* (111,112), Jones *et al.* (113) and Tademura *et al.* (114). However, except in rare circumstances, such as vitreous humor or CSF, it is probably not a suitable measure of absolute pO_2, since many factors can alter R_1 (115,116). We believe it can provide suitable evaluation of acute changes in pO_2.

We believe that combining BOLD and TOLD response to hyperoxic gas intervention provides particularly robust insight into tumor hypoxia and potential modulation. This is the basis of the simple test DOCENT (Dynamic Oxygen Challenge Evaluated by NMR T_1 and T_2*), as shown in Figure 9. To demonstrate the method, we chose a small HI tumor, which is known to be particularly well oxygenated and exhibit a large response to breathing hyperoxic gas (Table 3). We note a stable baseline for BOLD and a rapid response in signal intensity approaching 40% ΔSI within one minute of breathing carbogen (95% O_2, 5% CO_2) (Figure 9). Distinct heterogeneity was observed in any given slice, but quite similar data were seen by MRI in three adjacent tissue slices. The TOLD response was smaller and more sluggish, as expected, since O_2 must diffuse from the vasculature into the tumor tissue. Importantly, the combined methods robustly demonstrate delivery and accumulation of oxygen. It remains to be seen whether quantitative R_1 and R_2* measurements are required or simple R_1- and R_2*-weighted signal intensity changes will be useful. We are currently evaluating whether such measurements are predictive for radiation response in rat tumors. We are also implementing these methods in patients.

5 Innovations and latest applications

Within the past year, several innovations have been presented promising new insight into tumor hypoxia. There has been notable progress in quantitative oximetry based on ^{19}F MRI with new reports of applications. Gallez *et al.* implemented a faster imaging approach for ^{19}F MRI of hexafluorobenzene, Look-Locker type SNAP-IR measurements giving 90 s time resolution (117,118). Spatial resolution was similar to that previously reported for FREDOM (requiring 6.5 mins), though a larger volume of hexafluorobenzene reporter molecule was used (90 vs. 50 μl) and it remains to be seen whether the precision of measurements will be equivalent, since SNR is known to strongly influence the quality of relaxation rate measurements (78). We do ourselves sometimes use larger volumes of HFB in tumors, *e.g*. Figure 4. In any case, the faster temporal resolution opens new opportunities to explore rapid dynamic pO_2 fluctuations and transients: a new window on acute hypoxic episodes. Notably, both the groups in Louvain and UCSF are using ^{19}F MR oximetry of hexafluorobenzene to explore oxygen dynamics in response to pharmaceutical interventions (119–121). The use of HFB as a ^{19}F pO_2 reporter molecule is gaining popularity with new reports of applications. Diepart *et al*. have further used this technique to measure oxygen consumption in tumors (120). Using the FREDOM technique, Liu *et al*. (122) compared pO_2 changes in multiple organs during isovolemic anemic hemodilution using hemoglobin based oxygen carriers under normoxic and hyperoxic conditions in a rat model.

While we favor direct intra tumoral injection of HFB for immediate interrogation of regions of interest, we note a novel approach presented by Ahrens *et al*. (123). Several groups have pre-labeled cells in culture with PFC to allow cell tracking after implantation *in vivo* (124) *and* this has now been used to measure changes in intracellular pO_2 following implantation of cells.

Interrogation of hypoxia by NMR has received new impetus with the presentation of a trifluoronitroimidazole, which provided sufficient signal to noise to allow chemical shift imaging, as opposed to the more traditional signal limited spectroscopy (125). A novel approach uses a gadolinium liganded nitroimidazole (GdDO3NI), which showed increased MRI contrast in hypoxic central regions of rat prostate AT1 tumors compared to peripheral, well-perfused regions. Increased uptake of GdDO3NI in the tumor center was further confirmed by flame ionization spectroscopy post mortem (126).

Well characterized animal models exhibiting differential hypoxia are important for evaluating new methods of detecting hypoxia and evaluating novel therapies. Based on ^{19}F MRI, we have extensively characterized a series of Dunning prostate R3327 rat tumors, which exhibit a wide range of oxygen characteristics, as shown in Table 3. The Dunning prostate tumors have the great advantage of being syngeneic in rats allowing investigations in immunocompetent animals. Moreover, rats show much more stable physiology than mice under anesthesia and greater tumor burden is feasible. Indeed, knowledge of the hypoxia status was crucial in choosing a model to evaluate GdDO3NI

We find three distinct characteristics for tumor oxygenation and dynamics:

- **i.** hypoxic tumors, which do not respond to hyperoxic gas intervention;
- **ii.** hypoxic tumors, which do respond to hyperoxic gas intervention (*e.g.*, large HI, Figure 6);
- **iii.** well oxygenated tumors (*e.g.*, small HI, Figure 6). In every case examined to date, well oxygenated tumors became even better oxygenated with hyperoxic gas breathing.

6. Conclusions

Increasingly, there is evidence that hypoxia influences angiogenesis, tumor invasion and metastasis. Moreover, repeated bouts of intermittent hypoxic stress may be important in stimulating tumor progression. Thus, the ability to assess tumor oxygenation non-invasively, and repeatedly, with respect to acute or chronic interventions becomes increasingly important.

PET approaches are costly for small animal research, but they have already made the transition to clinical trials. They do require reporter molecules and suffer from the complications of radioactivity, notably substrate decay and waste disposal.

MRI approaches are very attractive for pre-clinical investigations of hypoxia and oxygen dynamics. They offer high spatial resolution, arbitrary tissue depth penetration and avoids complications of radioactivity. However, data acquisition is not trivial, throughput is quite modest and instrumentation is expensive. Uniquely, MRI can provide quantitative maps of pO_2 and reveal dynamic changes in response to interventions based on inert reporter molecules. ^{19}F MR oximetry, *e.g*., FREDOM, based on hexafluorobenzene is perfectly suited to measurements in pre-clinical animal studies providing quantitative pO_2 measurements with useful spatial and temporal resolution and precision relevant to radiotherapy (6). Given the well documented lack of toxicity clinical application ultimately

be feasible, but currently ^{19}F MRI remains esoteric on clinical MR scanners. PISTOL offers an analogous proton MRI approach (91). Repeat measurements of pO_2 are non-invasive, but both PISTOL and FREDOM approaches do require a reporter molecule.

Meanwhile, BOLD and TOLD MRI approaches offer entirely non-invasive assessments of tissue oxygenation dynamics and are clearly preferable for clinical applications. While they do not provide quantitative measurements of pO_2 there is increasing evidence that changes in R_1 and R_2* relate to changes in tissue and vascular oxygenation. Together the offer inter-dependant insight into tumor oxygenation and DOCENT (Dynamic Oxygen Challenge Evaluated by NMR T_1 and T_2*) promises to become a test for human tumor hypoxia and response to intervention based on the simple act of breathing oxygen during MRI.

Acknowledgments

This work was supported in part by the DOD Congressionally Directed Medical Research Programs DAMD#17-00-1-0437, W81XWH-08-1-0583, W81XWH-06-1-0475, W81XWH-06-1-0149, as well as NCI R01 CA139043-01A1 and 1R21 CA132096-01A1 in conjunction with Cancer Imaging Program SAIRP U24 CA126608 and NIH BRTP Facility P41-RR02584. We are grateful to Michael Long and Drs. Alex Hermanne, Xiankai Sun, Marc Jennewein and Frank Rösch for facilitating the radioarsenic study presented in Fig. 1d.

References

1. Gray L, Conger A, Ebert M, Hornsey S, Scott O. The concentration of oxygen dissolved in tissues at time of irradiation as a factor in radiotherapy. Br J Radiol 1953;26:638–648. [PubMed: 13106296]
2. Arbeit JM, Brown JM, Chao KS, Chapman JD, Eckelman WC, Fyles AW, Giaccia AJ, Hill RP, Koch CJ, Krishna MC, Krohn KA, Lewis JS, Mason RP, Melillo G, Padhani AR, Powis G, Rajendran JG, Reba R, Robinson SP, Semenza GL, Swartz HM, Vaupel P, Yang D, Croft B, Hoffman J, Liu G, Stone H, Sullivan D. Hypoxia: Importance in tumor biology, noninvasive measurement by imaging, and value of its measurement in the management of cancer therapy. Int J Radiat Biol 2006;82:699 – 757. [PubMed: 17118889]
3. Overgaard J, Horsman MR. Modification of hypoxia-induced radioresistance in tumors by the use of oxygen and sensitizers. Semin Radiat Oncol 1996;6:10–21. [PubMed: 10717158]
4. Moulder J, Rockwell S. Hypoxic fractions of solid tumors, experimental technique, methods of analysis and survey of existing data. Int J Radiat Oncol Biol Phys 1984;10:695–712. [PubMed: 6735758]
5. Dewhirst MW, Klitzman B, Braun RD, Brizel DM, Haroon ZA, Secomb TW. Review of methods used to study oxygen transport at the microcirculatory level. Int J Cancer 2000;90:237–255. [PubMed: 11091348]
6. Zhao D, Jiang L, Mason RP. Measuring Changes in Tumor Oxygenation. Methods Enzymol 2004;386:378–418. [PubMed: 15120262]
7. Swartz, HM.; Dunn, JF. Measurements of oxygen in tissues: overview and perspectives on methods. In: Dunn, JF.; Swartz, HM., editors. Oxygen Transport to Tissue XXIV. Vol. 530. New York: Kluwer Academic; 2003. p. 1-12.
8. Foo SS, Abbott DF, Lawrentschuk N, Scott AM. Functional imaging of intratumoral hypoxia. Molecular Imaging Biol 2004;6:291–305.
9. Yu, J-X.; Cui, W.; Zhao, D.; Mason, RP. Non-invasive physiology and pharmacology using ^{19}F magnetic resonance. In: Tressaud, A.; Haufe, G., editors. Fluorine and Health. Elsevier B.V; 2008. p. 198-276.
10. Knowles HJ, Harris AL. Hypoxia and oxidative stress in breast cancer. Hypoxia and tumourigenesis. Breast Cancer Res 2001;3:318–322. [PubMed: 11597321]
11. Graeber TG, Osmanian C, Jacks T, Housman DE, Koch CJ, Lowe SW, Giaccia AJ. Hypoxia-mediated selection of cells with diminished apoptotic potential in solid tumours. Nature 1996;379:88–91. [PubMed: 8538748]
12. Cairns RA, Kalliomaki T, Hill RP. Acute (cyclic) hypoxia enhances spontaneous metastasis of KHT murine tumors. Cancer Res 2001;61:8903–8908. [PubMed: 11751415]

13. Jain RK, Schlenger K, Höckel M, Yuan F. Quantitative angiogenesis assays: Progress and problem. Nature Med 1997;3:1203–1208. [PubMed: 9359693]
14. Ran S, Thorpe PE. Phosphatidylserine is a marker of tumor vasculature and a potential target for cancer imaging and therapy. Int J Radiat Oncol Biol Phys 2002;54:1479–1484. [PubMed: 12459374]
15. Jennewein M, Lewis M, Zhao D, Tsyganov T, Slavine N, He J, Watkins L, Kodibagkar V, O'Kelly S, Kulkarni P, Antich P, Hermanne A, Rösch F, Mason R, Thorpe P. Vascular imaging of solid tumors in rats with a radioactive arsenic-labeled antibody that binds exposed phosphatidylserine. Clin Cancer Res 2008;14:1377–1385. [PubMed: 18316558]
16. Rademakers SE, Span PN, Kaanders JHAM, Sweep FCGJ, van der Kogel AJ, Bussink J. Molecular aspects of tumour hypoxia. Molecular Oncology 2008;2:41–53. [PubMed: 19383328]
17. Krohn KA, Link JM, Mason RP. Molecular Imaging of Hypoxia. J Nucl Med 2008;49:129S–148S. [PubMed: 18523070]
18. Fomicheva EV, Turner II, Edwards TG, Hoff J, Arden E, D'Alecy LG, Metzger JM. Double oxygen-sensing vector system for robust hypoxia/ischemia-regulated gene induction in cardiac muscle in vitro and in vivo. Molecular Therapy 2008;16:1594–1601. [PubMed: 18578010]
19. Penet MF, Pathak AP, Raman V, Ballesteros P, Artemov D, Bhujwalla ZM. Noninvasive Multiparametric Imaging of Metastasis-Permissive Microenvironments in a Human Prostate Cancer Xenograft. Cancer Res 2009;69:8822–8829. [PubMed: 19861534]
20. Wouters BG, Brown JM. Cells at intermediate oxygen levels can be more important than the "hypoxic fraction" in determining tumor response to fractionated radiotherapy. Radiat Res 1997;147:541–550. [PubMed: 9146699]
21. Fowler JF, Tome WA, Fenwick JD, Mehta MP. A challenge to traditional radiation oncology. International Journal of Radiation Oncology Biology Physics 2004;60:1241–1256.
22. Timmerman RD, Paulus R, Galvin J, Michalski J, Straube W, Bradley J, Fakiris A, Bezjak A, Videtic G, Choy H. Stereotactic Body Radiation Therapy for Medically Inoperable Early-stage Lung Cancer Patients: Analysis of RTOG 0236. International Journal of Radiation Oncology*Biology*Physics 2009;75:S3–S3.
23. Flynn RT, Bowen SR, Bentzen SM, Mackie TR, Jeraj R. Intensity-modulated x-ray (IMXT) versus proton (IMPT) therapy for theragnostic hypoxia-based dose painting. Physics in Medicine and Biology 2008;53:4153–4167. [PubMed: 18635895]
24. Yang Y, Xing L. Towards biologically conformal radiation therapy (BCRT): Selective IMRT dose escalation under the guidance of spatial biology distribution. Medical Physics 2005;32:1473–1484. [PubMed: 16013703]
25. Malinen E, Sovik A, Hristov D, Bruland OS, Olsen DR. Adapting radiotherapy to hypoxic tumours. Physics in Medicine and Biology 2006;51:4903–4921. [PubMed: 16985278]
26. Thorwarth D, Eschmann SM, Paulsen F, Alber M. Hypoxia dose painting by numbers: A planning study. International Journal of Radiation Oncology Biology Physics 2007;68:291–300.
27. Albertella MR, Loadman PM, Jones PH, Phillips RM, Rarnpling R, Burnet N, Alcock C, Anthoney A, Vjaters E, Dunk CR, Harris PA, Wong A, Lalani AS, Twelves CJ. Hypoxia-selective targeting by the bioreductive prodrug AQ4N in patients with solid tumors: Results of a phase I study. Clinical Cancer Research 2008;14:1096–1104. [PubMed: 18281542]
28. Duan JX, Jiao H, Kaizerman J, Stanton T, Evans JW, Lan L, Lorente G, Banica M, Jung D, Wang J, Ma H, Li X, Yang Z, Hoffman RM, Ammons WS, Hart CP, Matteucci M. Potent and Highly Selective Hypoxia-Activated Achiral Phosphoramidate Mustards as Anticancer Drugs. Journal of Medicinal Chemistry 2008;51:2412–2420. [PubMed: 18257544]
29. Kaanders JHAM, Wijffels KIEM, Marres HAM, Ljungkvist ASE, Pop LAM, van den Hoogen FJA, de Wilde PCM, Bussink J, Raleigh JA, van der Kogel AJ. Pimonidazole binding and tumor vascularity predict for treatment outcome in head and neck cancer. Cancer Res 2002;62:7066–7074. [PubMed: 12460928]
30. Raleigh JA, Chou SC, Arteel GE, Horsman M. Comparison among pimonidazole binding, oxygen electrode measurements, and radiation response in C3H mouse tumors. Radiat Res 1999;151:580–589. [PubMed: 10319731]

31. Dolbier WR Jr, Li AR, Koch CJ, Shiue CY, Kachur AV. [18F]-EF5, a marker for PET detection of hypoxia: synthesis of precursor and a new fluorination procedure. Appl Radiat Isotop 2001;54:73–80.
32. Evans SM, Hahn S, Pook DR, Jenkins WT, Chalian AA, Zhang P, Stevens C, Weber R, Weinstein G, Benjamin I, Mirza N, Morgan M, Rubin S, McKenna WG, Lord EM, Koch CJ. Detection of hypoxia in human squamous cell carcinoma by EF5 binding. Cancer Res 2000;60:2018–2024. [PubMed: 10766193]
33. Ljungkvist ASE, Bussink J, Rijken PFJW, Raleigh JA, Denekamp J, Van Der Kogel AJ. Changes in tumor hypoxia measured with a double hypoxic marker technique. Int J Radiat Oncol Biol Phys 2000;48:1529–1538. [PubMed: 11121659]
34. Dehdashti F, Mintun MA, Lewis JS, Bradley J, Govinda R, Laforest R, Welch MJ, Siegel BA. In vivo assessment of tumor hypoxia in lung cancer with (60)Cu-ATSM. Eur J Nucl Med Molec Imaging 2003;30:844–850. [PubMed: 12692685]
35. Chapman JD, Engelhardt EL, Stobbe CC, Schneider RF, Hanks GE. Measuring hypoxia and predicting tumor radioresistance with nuclear medicine assays. Radiother Oncol 1998;46:229–237. [PubMed: 9572615]
36. Koch CJ. Measurement of absolute oxygen levels in cells and tissues using oxygen sensors and 2 - nitroimidazole EF5. Methods Enzymol 2002;352:3–31. [PubMed: 12125356]
37. Dehdashti F, Grigsby PW, Mintun MA, Lewis JS, Siegel BA, Welch MJ. Assessing tumor hypoxia in cervical cancer by positron emission tomography with 60Cu-ATSM: relationship to therapeutic response-a preliminary report. Int J Radiat Oncol Biol, Phys 2003;55:1233–1238. [PubMed: 12654432]
38. Robinson SP, Griffiths JR. Current issues in the utility of ^{19}F nuclear magnetic resonance methodologies for the asssessment of tumour hypoxia. Phil Trans R Soc London B Biol Sci 2004;359:987–996. [PubMed: 15306411]
39. Maxwell RJ, Workman P, Griffiths JR. Demonstration of tumor-selective retention of fluorinated nitroimidazole probes by ^{19}F magnetic resonance spectroscopy *in vivo*. Int J Radiat Oncol Biol Phys 1989;16:925–929. [PubMed: 2703398]
40. Ballinger JR. Imaging hypoxia in tumors. Semin Nucl Med 2001;31:321–329. [PubMed: 11710774]
41. Fang SW, Hong MT, Zhang H. Positron Emission Tomography Imaging of Tumor Hypoxia. Current Medical Imaging Reviews 2010;6:8–16.
42. Mees G, Dierckx R, Vangestel C, Van de Wiele C. Molecular imaging of hypoxia with radiolabelled agents. European Journal of Nuclear Medicine and Molecular Imaging 2009;36:1674–1686. [PubMed: 19565239]
43. Reischl G, Dorow DS, Cullinane C, Katsifis A, Roselt P, Binns D, Hicks RJ. Imaging of tumor hypoxia with [I-124] IAZA in comparison with [F-18] FMISO and [F-18]FAZA - first small animal PET results. Journal of Pharmacy and Pharmaceutical Sciences 2007;10:203–211. [PubMed: 17706178]
44. Riedl C, Brader P, Zanzonico P, Reid V, Woo Y, Wen B, Ling C, Hricak H, Fong Y, Humm J. Tumor hypoxia imaging in orthotopic liver tumors and peritoneal metastasis: a comparative study featuring dynamic 18F-MISO and 124I-IAZG PET in the same study cohort. European Journal of Nuclear Medicine and Molecular Imaging 2008;35:39–46. [PubMed: 17786438]
45. McQuade PJ, RD, Lewis JS, Welch MJ. Positron-Emitting Isotopes Produced on Biomedical Cyclotrons. Curr Med Chem 2005;12:807–818. [PubMed: 15853713]
46. Liu J, Hajibeigi A, Ren G, Lin M, Siyambalapitiyage W, Liu ZS, Simpson E, Parkey RW, Sun XK, Oz OK. Retention of the Radiotracers Cu-64-ATSM and Cu-64-PTSM in Human and Murine Tumors Is Influenced by MDR1 Protein Expression. Journal of Nuclear Medicine 2009;50:1332–1339. [PubMed: 19617332]
47. O'Donoghue JA, Zanzonico P, Pugachev A, Wen BX, Smith-Jones P, Cai SD, Burnazi E, Finn RD, Burgman P, Ruan S, Lewis JS, Welch MJ, Ling CC, Humm JL. Assessment of regional tumor hypoxia using F-18-fluoromisonidazole and Cu-64(II)-diacetyl-bis(N4-methylthiosemicarbazone) positron emission tomography: Comparative study featuring microPET imaging, Po-2 probe

measurement, autoradiography, and fluorescent microscopy in the R3327-AT and FaDu rat tumor models. International Journal of Radiation Oncology Biology Physics 2005;61:1493–1502.

48. Lewis JS, Laforest R, Dehdashti F, Grigsby PW, Welch MJ, Siegel BA. An Imaging Comparison of 64Cu-ATSM and 60Cu-ATSM in Cancer of the Uterine Cervix. J Nucl Med 2008;49:1177–1182. [PubMed: 18552145]
49. Jennewein M, Hermanne A, Mason RP, Thorpe PE, Rösch F. A new method for the labelling of proteins with radioactive arsenic isotopes. Nuclear Instruments and Methods in Physics Research Section A: Accelerators, Spectrometers, Detectors and Associated Equipment 2006;569:512–517.
50. Cherk MH, Foo SS, Poon AMT, Knight SR, Murone C, Papenfuss AT, Sachinidis JI, Saunder THC, O'Keefe GJ, Scott AM. Lack of correlation of hypoxic cell fraction and angiogenesis with glucose metabolic rate in non-small cell lung cancer assessed by F-18-fluoromisonidazole and F-18-FDG PET. Journal of Nuclear Medicine 2006;47:1921–1926. [PubMed: 17138734]
51. Swartz HM. Measuring real levels of oxygen in vivo: opportunities and challenges. Biochem Soc Trans 2002;30:248–252. [PubMed: 12023859]
52. Cater D, Silver I. Quantitative measurements of oxygen tension in normal tissues and in the tumors of patients before and after radiotherapy. Acta Radiol 1960;53:233–256. [PubMed: 13808406]
53. Fyles A, Milosevic M, Pintilie M, Syed A, Levin W, Manchul L, Hill RP. Long-term performance of interstial fluid pressure and hypoxia as prognostic factors in cervix cancer. Radiother Oncol 2006;80:132–137. [PubMed: 16920212]
54. Brizel DM, Sibly GS, Prosmitz LR, Scher RL, Dewhirst MW. Tumor hypoxia adversely affects the prognosis of carcinoma of the head and neck. Int J Radiat Oncol Biol Phys 1997;38:285–289. [PubMed: 9226314]
55. Höckel M, Schlenger K, Aral B, Mitze M, Schäffer U, Vaupel P. Association between tumor hypoxia and malignant progression in advanced cancer of the uterine cervix. Cancer Res 1996;56:4509–4515. [PubMed: 8813149]
56. Fyles A, Milosevic M, Hedley D, Pintilie M, Levin W, Manchul L, Hill RP. Tumor hypoxia has independent predictor impact only in patients with node-negative cervix cancer. J Clin Oncol 2002;20:680–687. [PubMed: 11821448]
57. Fyles AW, Milosevic M, Wong R, Kavanagh MC, Pintile M, Sun A, Chapman W, Levin W, Manchul L, Keane TJ, Hill RP. Oxygenation predicts radiation response and survival in patients with cervix cancer. Radiother Oncol 1998;48:149–156. [PubMed: 9783886]
58. Yeh KA, Biade S, Lanciano RM, Brown DQ, Fenning MC, Babb JS, Hanks GE, Chapman JD. Polarographic Needle Electrode Measurements of Oxygen in Rat Prostate Carcinomas: Accuracy and Reproducibility. Int J Radiat Oncol Biol Phys 1995;33:111–118. [PubMed: 7642408]
59. Aquino-Parsons C, Green A, Minchinton AI. Oxygen tension in primary gynaecological tumours: the influence of carbon dioxide concentration. Radiother Oncol 2000;57:45–51. [PubMed: 11033188]
60. Partridge SE, Aquino-Parsons C, Luo C, Green A, Olive PL. A pilot study comparing intratumoral oxygenation using the comet assay following 2.5% and 5% carbogen and 100% oxygen. International Journal of Radiation Oncology*Biology*Physics 2001;49:575–580.
61. Gu Y, Bourke V, Kim JG, Constantinescu A, Mason RP, Liu H. Dynamic Response of Breast Tumor Oxygenation to Hyperoxic Respiratory Challenge Monitored with Three Oxygen-Sensitive Parameters. Applied Optics 2003;42:1–8.
62. Zhao D, Constantinescu A, Hahn EW, Mason RP. Tumor oxygen dynamics with respect to growth and respiratory challenge: investigation of the Dunning prostate R3327-HI tumor. Radiat Res 2001;156:510–520. [PubMed: 11604064]
63. Jordan BF, Beghein N, Aubry M, Gregoire V, Gallez B. Potentiation of radiation-induced regrowth delay by isosorbide dinitrate in FSaII murine tumors. Int J Cancer 2003;103:138–141. [PubMed: 12455068]
64. Kuppusamy P, Afeworki R, Shankar RA, Coffin D, Krishna MC, Hahn SM, Mitchell JB, Zweier JL. In vivo electron paramagnetic resonance imaging of tumor heterogeneity and oxygenation in a murine model. Cancer Res 1998;58:1562–1568. [PubMed: 9537265]
65. Elas M, Williams BB, Parasca A, Mailer C, Pelizzari CA, Lewis MA, River JN, Karczmar GS, Barth ED, Halpern HJ. Quantitative tumor oxymetric images from 4D electron paramagnetic

resonance imaging (EPRI): Methodology and comparison with blood oxygen level-dependent (BOLD) MRI. Magn Reson Med 2003;49:682–691. [PubMed: 12652539]

66. O'Hara JA, Goda F, Demidenko E, Swartz HM. Effect on regrowth delay in a murine tumor of scheduling split-dose irradiation based on direct pO_2 measurements by electron paramagnetic resonance oximetry. Radiat Res 1998;150:549–556. [PubMed: 9806597]
67. Gallez B, Jordan BF, Baudelet C, Misson PD. Pharmacological modifications of the partial pressure of oxygen in murine tumors: Evaluation using in vivo EPR oximetry. Magn Reson Med 1999;42:627–630. [PubMed: 10502749]
68. Liu H, Song Y, Worden KL, Jiang X, Constantinescu A, Mason RP. Noninvasive Investigation of Blood Oxygenation Dynamics of Tumors by Near-Infrared Spectroscopy. Appl Optics 2000;39:5231–5243.
69. Gallez B, Baudelet C, Jordan BF. Assessment of tumor oxygenation by electron paramagnetic resonance: principles and applications. NMR Biomed 2004;17:240 – 262. [PubMed: 15366026]
70. Kodibagkar VD, Wang X, Mason RP. Physical principles of quantitative nuclear magnetic resonance oximetry. Front Biosci 2008;13:1371–1384. [PubMed: 17981636]
71. Harris AL. Hypoxia--a key regulatory factor in tumour growth. Nat Rev Cancer 2002;2:38 – 47. [PubMed: 11902584]
72. Morse DL, Gillies RJ. Molecular imaging and targeted therapies. Biochemical Pharmacology. In Press, Corrected Proof.
73. Rischin D, Hicks RJ, Fisher R, Binns D, Corry J, Porceddu S, Peters LJ. Prognostic Significance of [18F]-Misonidazole Positron Emission Tomography-Detected Tumor Hypoxia in Patients With Advanced Head and Neck Cancer Randomly Assigned to Chemoradiation With or Without Tirapazamine: A Substudy of Trans-Tasman Radiation Oncology Group Study 98.02. J Clin Oncol 2006;24:2098–2104. [PubMed: 16648512]
74. Mason RP. Non-invasive physiology: ^{19}F NMR of perfluorocarbon. Art Cells, Blood Sub & Immob Biotech 1994;22:1141–1153.
75. Mason RP, Shukla HP, Antich PP. *In vivo* oxygen tension and temperature: Simultaneous determination using ^{19}F spectroscopy of perfluorocarbon. Magn Reson Med 1993;29:296–302. [PubMed: 8450738]
76. Mason RP, Antich PP, Babcock EE, Constantinescu A, Peschke P, Hahn EW. Non-invasive determination of tumor oxygen tension and local variation with growth. Int J Radiat Oncol Biol Phys 1994;29:95–103. [PubMed: 8175452]
77. Dardzinski BJ, Sotak CH. Rapid tissue oxygen tension mapping using ^{19}F Inversion-recovery Echo-planar imaging of Perfluoro-15-crown-5-ether. Magn Reson Med 1994;32:88–97. [PubMed: 8084241]
78. Barker BR, Mason RP, Bansal N, Peshock RM. Oxygen tension mapping by ^{19}F echo planar NMR imaging of sequestered perfluorocarbon. JMRI 1994;4:595–602. [PubMed: 7949687]
79. Mason, RP.; Hunjan, S.; Constantinescu, A.; Song, Y.; Zhao, D.; Hahn, EW.; Antich, PP.; Peschke, P. Tumor oximetry: Comparison of ^{19}F MR EPI and electrodes. In: Dunn, JF.; Swartz, HM., editors. Oxygen Transport to Tissue XXIV. Vol. 530. New York: Kluwer; 2003. p. 19-28.
80. Kim JG, Zhao D, Constantinescu A, Mason RP, Liu H. Interplay of Tumor Vascular Oxygenation and Tumor pO_2 Observed Using NIRS, Oxygen Needle Electrode, and ^{19}F MR pO_2 Mapping. J. Biomed. Optics 2003;8:53–62.
81. Zhao D, Ran S, Constantinescu A, Hahn EW, Mason RP. Tumor oxygen dynamics: correlation of in vivo MRI with histological findings. Neoplasia 2003;5:308–318. [PubMed: 14511402]
82. Xia M, Kodibagkar V, Liu H, Mason RP. Tumour oxygen dynamics measured simultaneously by near infrared spectroscopy and ^{19}F magnetic resonance imaging in rats. Phys Med Biol 2006;51:45–60. [PubMed: 16357430]
83. Hunjan S, Mason RP, Constantinescu A, Peschke P, Hahn EW, Antich PP. Regional tumor oximetry: ^{19}F NMR spectroscopy of hexafluorobenzene. Int J Radiat Oncol Biol Phys 1998;40:161–171. [PubMed: 9588931]
84. Zhao D, Constantinescu C, Hahn EW, Mason RP. Differential oxygen dynamics in two diverse Dunning prostate R3327 rat tumor sublines (MAT-Lu and HI) with respect to growth and respiratory challenge. Int J Radiat Oncol Biol Phys 2002;53:744–756. [PubMed: 12062621]

85. Zhao D, Constantinescu A, Chang CH, Hahn EW, Mason RP. Correlation of Tumor Oxygen Dynamics with Radiation Response of the Dunning Prostate R3327-HI Tumor. Radiat Res 2003;159:621–631. [PubMed: 12710873]
86. Bourke VA, Zhao D, Gilio J, Chang CH, Jiang L, Hahn EW, Mason RP. Correlation of Radiation Response with Tumor Oxygenation in the Dunning Prostate R3327-AT1 Tumor. Int J Radiat Oncol Biol Phys 2007;67:1179–1186. [PubMed: 17336219]
87. Xia, M.; Liu, H.; Ren, Y.; Mason, R.; Levine, B. Simultaneous monitoring of tumor vascular and tissue oxygen tension under hyperbaric oxygen exposure. Biomedical Optics Topical Meeting; Fort Lauderdale, Florida. 2006.
88. Zhao D, Constantinescu A, Jiang L, Hahn EW, Mason RP. Prognostic Radiology: quantitative assessment of tumor oxygen dynamics by MRI. Am J Clin Oncol 2001;24:462–466. [PubMed: 11586097]
89. Zhao D, Jiang L, Hahn EW, Mason RP. Tumor physiological response to combretastatin A4 phosphate assessed by MRI. Int J Radiat Oncol Biol Phys 2005;62:872–880. [PubMed: 15936572]
90. Kodibagkar VD, Cui W, Merritt ME, Mason RP. A novel ^{1}H NMR approach to quantitative tissue oximetry using hexamethyldisiloxane. Magn Reson Med 2006;55:743–748. [PubMed: 16506157]
91. Kodibagkar VD, Wang X, Pacheco-Torres J, Gulaka P, Mason RP. Proton Imaging of Siloxanes to map Tissue Oxygenation Levels (PISTOL): a tool for quantitative tissue oximetry. NMR Biomed 2008;21:899–907. [PubMed: 18574806]
92. Howe FA, Robinson SP, McIntyre DJ, Stubbs M, Griffiths JR. Issues in flow and oxygenation dependent contrast (FLOOD) imaging of tumours. NMR Biomed 2001;14:497–506. [PubMed: 11746943]
93. Xu F, Ge YL, Lu HZ. Noninvasive Quantification of Whole-Brain Cerebral Metabolic Rate of Oxygen (CMRO2) by MRI. Magnetic Resonance in Medicine 2009;62:141–148. [PubMed: 19353674]
94. Wright GA, Hu BS, Macovski A. Estimating oxygen saturation of blood in vivo with MR imaging at 1.5 T. JMRI 1991;1:275–283. [PubMed: 1802140]
95. He X, Yablonskiy DA. Quantitative BOLD: Mapping of human cerebral deoxygenated blood volume and oxygen extraction fraction: Default state. Magnetic Resonance in Medicine 2007;57:115–126. [PubMed: 17191227]
96. Robinson SP, Rijken PF, Howe FA, McSheehy PM, van der Sanden BP, Heerschap A, Stubbs M, Van Der Kogel AJ, Griffiths JR. Tumor vascular architecture and function evaluated by non-invasive susceptibility MRI methods and immunohistochemistry. J Magn Reson Imaging 2003;17:445–454. [PubMed: 12655584]
97. Griffiths JR, Taylor NJ, Howe FA, Saunders MI, Robinson SP, Hoskins PJ, Powell MEB, Thoumine M, Caine LA, Baddeley H. The response of human tumors to carbogen breathing monitored by gradient-recalled echo MRI. Int J Radiat Oncol Biol Phys 1997;39:697–701. [PubMed: 9336152]
98. Al-Hallaq HA, River JN, Zamora M, Oikawa H, Karczmar GS. Correlation of magnetic resonance and oxygen microelectrode measurements of carbogen-induced changes in tumor oxygenation. Int J Radiat Oncol Biol Phys 1998;41:151–159. [PubMed: 9588930]
99. Dunn JF, O'Hara JA, Zaim-Wadghiri Y, Lei H, Meyerand ME, Grinberg OY, Hou H, Hoopes PJ, Demidenko E, Swartz HM. Changes in oxygenation of intracranial tumors with carbogen: a BOLD MRI and EPR oximetry study. JMRI 2002;16:511–521. [PubMed: 12412027]
100. Zhao D, Lan JL, Hahn EW, Mason RP. Comparison of ^{1}H blood oxygen level-dependent (BOLD) and ^{19}F MRI to investigate tumor oxygenation. Magnetic Resonance in Medicine 2009;62:357–364. [PubMed: 19526495]
101. Baudelet C, Gallez B. Current issues in the utility of blood oxygen level dependent MRI for the assessment of modulations in tumor oxygenation. Curr Med Imaging Rev 2005;1:229–243.
102. Baudelet C, Gallez B. How does blood oxygen level-dependent (BOLD) contrast correlate with oxygen partial pressure (pO_2) inside tumors? Magn Reson Med 2002;48:980–986. [PubMed: 12465107]

103. Taylor NJ, Baddeley H, Goodchild KA, Powell ME, Thoumine M, Culver LA, Stirling JJ, Saunders MI, Hoskin PJ, Phillips H, Padhani AR, Griffiths JR. BOLD MRI of human tumor oxygenation during carbogen breathing. JMRI 2001;14:156–163. [PubMed: 11477674]

104. Padhani A, Krohn K, Lewis J, Alber M. Imaging oxygenation of human tumours. Europ Radiol 2007;17:861–872.

105. Hoskin PJ, Carnell DM, Taylor NJ, Smith RE, Stirling JJ, Daley FM, Saunders MI, Bentzen SM, Collins DJ, d'Arcy JA, Padhani AP. Hypoxia in Prostate Cancer: Correlation of BOLD-MRI With Pimonidazole Immunohistochemistry--Initial Observations. International Journal of Radiation Oncology*Biology*Physics 2007;68:1065–1071.

106. Rodrigues LM, Howe FA, Griffiths JR, Robinson SP. Tumor R-2 * is a prognostic indicator of acute radiotherapeutic response in rodent tumors. Journal of Magnetic Resonance Imaging 2004;19:482–488. [PubMed: 15065173]

107. Gullino PM, Granthan FH, Courtney AH. Utilization of oxygen by transplanted tumors in vivo. Cancer Res 1967;27:1020–1029. [PubMed: 4290856]

108. Vaupel, P. Atemgaswechsel und Glucosestoffwechsel von Implantationstumoren (DS-Carcinosarkom)*in vivo*. Vol. 1. Mainz: Akademie der Wissenschaften und der Literatur; 1974. p. 5-138.

109. Matsumoto K, Bernardo M, Subramanian S, Choyke P, Mitchell JB, Krishna MC, Lizak MJ. MR assessment of changes of tumor in response to hyperbaric oxygen treatment. Magn Reson Med 2006;56:240–246. [PubMed: 16795082]

110. Edelman RR, Hatabu H, Tadamura E, Li W, Prasad PV. Noninvasive assessment of regional ventilation in the human lung using oxygen-enhanced magnetic resonance imaging. Nature Medicine 1996;2:1236–1239.

111. O'Connor JPB, Jackson A, Buonaccorsi GA, Buckley DL, Roberts C, Watson Y, Cheung S, McGrath DM, Naish JH, Rose CJ, Dark PM, Jayson GC, Parker GJM. Organ-specific effects of oxygen and carbogen gas inhalation on tissue longitudinal relaxation times. Magn Reson Med 2007;58:490–496. [PubMed: 17763345]

112. O'Connor JPB, Naish JH, Jackson A, Waterton JC, Watson Y, Cheung S, Buckley DL, McGrath DM, Buonaccorsi GA, Mills SJ, Roberts C, Jayson GC, Parker GJM. Comparison of Normal Tissue R-1 and R-2* Modulation by Oxygen and Carbogen. Magnetic Resonance in Medicine 2009;61:75–83. [PubMed: 19097212]

113. Jones RA, Ries M, Moonen CTW, Grenier N. Imaging the changes in renal T-1 induced by the inhalation of pure oxygen: A feasibility study. Magnetic Resonance in Medicine 2002;47:728–735. [PubMed: 11948734]

114. Tadamura E, Hatabu H, Li W, Prasad PV, Edelman RR. Effect of oxygen inhalation on relaxation times in various tissues. J Magn Reson Imaging 1997;7:220–225. [PubMed: 9039619]

115. Berkowitz BA, McDonald C, Ito Y, Tofts PS, Latif Z, Gross J. Measuring the human retinal oxygenation response to a hyperoxic challenge using MRI: eliminating blinking artifacts and demonstrating proof of concept. Magn Reson Med 2001;46:412–416. [PubMed: 11477648]

116. Lewa CJ, Majewska Z. Temperature relationships of proton spin-lattice relaxation time T1 in biological tissues. Bull Cancer 1980;67:35.

117. Jordan BF, Cron GO, Gallez B. Rapid monitoring of oxygenation by ^{19}F magnetic resonance imaging: Simultaneous comparison with fluorescence quenching. Magn Reson Med 2009;61:634–638. [PubMed: 19097235]

118. Liu, S.; Wilmes, LJ.; Kodibagkar, V.; Hylton, N.; Hopf, H.; Mason, RP.; Rollins, MD. Preliminary Studies of Quantitative Tissue Oxygen Measurement in Multiple Organs Using ^{19}F MRI. 16th ISMRM; Toronto, Canada. 2008. p. 197

119. Liu, S.; Shah, SJ.; Wilmes, LJ.; Kodibagkar, V.; Wendland, MF.; Hylton, N.; Hopf, HW.; Mason, RP.; Rollins, MD. Evaluation of severe anemia by quantitatively measuring multi-organ oxygen using ^{19}F MRI in a rat model. Proc. ISMRM; Honolulu, HI. 2009.

120. Diepart, C.; Karroum, O.; Magat, J.; Feron, O.; Jordan, B.; Gallez, B. MR characterization of the tumor microenvironment after arsenic trioxide treatment: evidence for an effect on oxygen consumption that radiosensitizes solid tumors. Proc. Joint ISMRM- ESMRMB; 2010.

121. Jordan, BF.; Peeterbroeck, J.; Karroum, O.; Diepart, C.; Magat, J.; Gregoire, V.; Gallez, B. Captopril and S-nitrosocaptopril as potent radiosensitizers: Comparative MR study and underlying mechanisms. Proc Joint ISMRM-ESMRMB; Stockholm, Sweden. 2010.

122. Liu, S.; Shah, SJ.; Wilmes, LJ.; Kodibagkar, VD.; Wendland, MF.; Apfel, CC.; Hylton, NM.; Hopf, H.; Mason, RP.; Rollins, MD. Evaluation of artificial blood substitutes by quantitatively measuring multi-organ oxygen using ^{19}F MRI in a rat model; ISMRM; Stockholm, Sweden: 2010.

123. Kadayakkara, DK.; Pusateri, LK.; Xu, J.; Janjic, JM.; Ahrens, ET. In vivo intracellular pO_2 measurements of perfluorocarbon labeled 9L glioma cells. Proc. 16th Intl. Soc. Mag. Reson. Med; Toronto, Canada. 2008. p. 800

124. Wickline, SA.; Mason, RP.; Caruthers, SD.; Chen, J.; Winter, PM.; Hughes, MS.; Lanza, GM. Fluorocarbon Agents for Quantitative Multimodal Molecular Imaging and Targeted Therapeutics. Weissleder, R.; Gambhir, SS.; Ross, BD.; Rehemtulla, A., editors. Hamilton, Ontario, Canada: BC Decker Inc; 2010. in the press

125. Procissi D, Claus F, Burgman P, Koziorowski J, Chapman JD, Thakur SB, Matei C, Ling CC, Koutcher JA. In vivo F-19 magnetic resonance spectroscopy and chemical shift imaging of tri-fluoro-nitroimidazole as a potential hypoxia reporter in solid tumors. Clinical Cancer Res 2007;13:3738–3747. [PubMed: 17575240]

126. Kodibagkar, VD.; Gulaka, PK.; Rojas-Quinjano, F.; Kovacs, ZPMR.; Sherry, AD. In vitro and in vivo evaluation of GdDO3NI as a hypoxia targeting MRI T1 contrast agent. Proc. ISMRM; Stockholm, Sweden. 2010.

127. Jiang L, Zhao D, Constantinescu A, Mason RP. Comparison of BOLD contrast and Gd-DTPA Dynamic Contrast Enhanced imaging in rat prostate tumor. Magn Reson Med 2004;51:953–960. [PubMed: 15122677]

128. O'Connor JPB, Naish JH, Parker GJM, Waterton JC, Watson Y, Jayson GC, Buonaccorsi GA, Cheung S, Buckley DL, McGrath DM, West CML, Davidson SE, Roberts C, Mills SJ, Mitchell CL, Hope L, Ton C, Jackson A. Preliminary Study of Oxygen-Enhanced Longitudinal Relaxation in Mri: a Potential Novel Biomarker of Oxygenation Changes in Solid Tumors. International Journal of Radiation Oncology Biology Physics 2009;75:1209–1215.

129. Fan X, River JN, Zamora M, Al-Hallaq HA, Karczmar GS. Effect of carbogen on tumor oxygenation: combined fluorine-19 and proton MRI measurements. Int J Radiat Oncol Biol Phys 2002;54:1202–1209. [PubMed: 12419449]

130. McIntyre DJO, McCoy CL, Griffiths JR. Tumour oxygenation measurements by ^{19}F MRI of perfluorocarbons. Curr Sci 1999;76:753–762.

131. Wang Z, Su MY, Nalcioglu O. Applications of Dynamic Contrast Enhanced MRI in Oncology: Measurement of Tumor Oxygen Tension. Technol Cancer Res Treat 2002;1:29–38. [PubMed: 12614174]

132. Cooper RA, Carrington BM, Loncasters JA, Todd SM, Davidson SE, Logue JP, Luthra AD, Jones AP, Stratford I, Hunter RD, West CML. Tumour oxygenation levels correlate with dynamic contrast-enhanced magnetic resonance imaging parameters in carcinoma of the cervix. Radiother Oncol 2000;57:53–59. [PubMed: 11033189]

133. Lyng H, Vorren AO, Sundfor K, Taksdal I, Lien HH, Kaalhus O, Rofstad EK. Assessment of tumor oxygenation in human cervical carcinoma by use of dynamic Gd-DTPA-enhanced MR imaging. JMRI 2001;14:750–756. [PubMed: 11747032]

134. Wilson D, Cerniglia G. Localization of tumors and evaluation of their state of oxygenation by phosphorescence imaging. Cancer Res 1992;52:3988–3993. [PubMed: 1617675]

135. Pogue BW, Zhu H, Nwaigwe C, McBride TO, Osterberg UL, Paulsen KD, Dunn JF. Hemoglobin imaging with hybrid magnetic resonance and near-infrared diffuse tomography. Adv Exp Med Biol 2003;530:215–224. [PubMed: 14562719]

136. Adamsen TCH, Grierson JR, Krohn KA. A new synthesis of the labeling precursor for [F-18]-fluoromisonidazole. Journal of Labelled Compounds & Radiopharmaceuticals 2005;48:923–927.

137. Rasey JS, Koh WJ, Grierson JR, Grunbaum Z, Krohn KA. Radiolabeled fluoromisonidazole as an imaging agent for tumor hypoxia. International Journal of Radiation Oncology*Biology*Physics 1989;17:985–991.

138. Lee ST, Scott AM. Hypoxia Positron Emission Tomography Imaging With 18F-Fluoromisonidazole. Seminars in Nuclear Medicine 2007;37:451–461. [PubMed: 17920352]
139. Kachur AV, DolbierJr WR, Evans SM, Shiue CY, Shiue GG, Skov KA, Baird IR, James BR, Li AR, Roche A, Koch CJ. Synthesis of new hypoxia markers EF1 and [18F]-EF1. Applied Radiation and Isotopes 1999;51:643–650. [PubMed: 10581679]
140. Evans SM, Kachur AV, Shiue CY, Hustinx R, Jenkins WT, Shive GG, Karp JS, Alavi A, Lord EM, Dolbier WR, Koch CJ. Noninvasive detection of tumor hypoxia using the 2-nitroimidazole [F-18]EF1. Journal of Nuclear Medicine 2000;41:327–336. [PubMed: 10688119]
141. Josse O, Labar D, Georges B, Gregoire V, Marchand-Brynaert J. Synthesis of [F-18]-labeled EF3 [2-(2-nitroimidazol-1-yl)-N-(3,3,3-trifluoropropyl)-acetamide], a marker for PET detection of hypoxia. Bioorganic & Medicinal Chemistry 2001;9:665–675. [PubMed: 11310602]
142. Dubois L, Landuyt W, Cloetens L, Bol A, Bormans G, Haustermans K, Labar D, Nuyts J, Gregoire V, Mortelmans L. [F-18]EF3 is not superior to [F-18]FMISO for PET-based hypoxia evaluation as measured in a rat rhabdomyosarcoma tumour model. European Journal of Nuclear Medicine and Molecular Imaging 2009;36:209–218. [PubMed: 18690432]
143. Mahy P, Geets X, Lonneux M, Leveque P, Christian N, De Bast M, Gillart J, Labar D, Lee J, Gregoire V. Determination of tumour hypoxia with [F-18]EF3 in patients with head and neck tumours: a phase I study to assess the tracer pharmacokinetics, biodistribution and metabolism. European Journal of Nuclear Medicine and Molecular Imaging 2008;35:1282–1289. [PubMed: 18317752]
144. Dolbier WR, Li AR, Koch CJ, Shiue CY, Kachur AV. [F-18]-EF5, a marker for PET detection of hypoxia: synthesis of precursor and a new fluorination procedure. Applied Radiation and Isotopes 2001;54:73–80. [PubMed: 11144255]
145. Evans SM, Joiner B, Jenkins WT, Laughlin KM, Lord EM, Koch CJ. Identification of Hypoxia in Cells and Tissues of Epigastric 9l Rat Glioma Using Ef5 [2-(2-Nitro-1h-Imidazol-1-Yl)-N-(2,2,3,3,3-Pentafluoropropyl) Acetamide]. British Journal of Cancer 1995;72:875–882. [PubMed: 7547234]
146. Koch CJ, Shuman AL, Jenkins WT, Kachur AV, Karp JS, Freifelder R, Dolbier WR, Evans SM. The radiation response of cells from 9L gliosarcoma tumours is correlated with [F18]-EF5 uptake. International Journal of Radiation Biology 2009;85:1137–1147. [PubMed: 19995239]
147. Komar G, Seppanen M, Eskola O, Lindholm P, Gronroos TJ, Forsback S, Sipila H, Evans SM, Solin O, Minn H. F-18-EF5: A New PET Tracer for Imaging Hypoxia in Head and Neck Cancer. Journal of Nuclear Medicine 2008;49:1944–1951. [PubMed: 18997048]
148. Tewson TJ. Synthesis of [F-18]fluoroetanidazole: A potential new tracer for imaging hypoxia. Nuclear Medicine and Biology 1997;24:755–760. [PubMed: 9428602]
149. Barthel H, Wilson H, Collingridge DR, Brown G, Osman S, Luthra SK, Brady F, Workman P, Price PM, Aboagye EO. In vivo evaluation of [F-18]fluoroetanidazole as a new marker for imaging tumour hypoxia with positron emission tomography. British Journal of Cancer 2004;90:2232–2242. [PubMed: 15150578]
150. Yang DJ, Wallace S, Cherif A, Li C, Gretzer MB, Kim EE, Podoloff DA. Development of F-18-labeled fluoroerythronitroimidazole as a PET agent for imaging tumor hypoxia. Radiology 1995;194:795–800. [PubMed: 7862981]
151. Yang DJ, Wallace S, Cherif A, Li C, Gretzer MB, Kim EE, Podoloff DA. Development of F-18 Labeled Fluoroerythronitroimidizole as a Pet Agent for Imaging Tumor Hypoxia. Radiology 1995;194:795–800. [PubMed: 7862981]
152. Lehtio K, Oikonen V, Nyman S, Gronroos T, Roivainen A, Eskola I, Minn H. Quantifying tumour hypoxia with fluorine-18 fluoroerythronitroimidazole([F-18]FETNIM) and PET using the tumour to plasma ratio. European Journal of Nuclear Medicine and Molecular Imaging 2003;30:101–108. [PubMed: 12483416]
153. Reischl G, Ehrlichmann W, Bieg C, Solbach C, Kumar P, Wiebe LI, Machulla HJ. Preparation of the hypoxia imaging PET tracer [18F]FAZA: reaction parameters and automation. Applied Radiation and Isotopes 2005;62:897–901. [PubMed: 15799867]

154. Piert M, Machulla HJ, Picchio M, Reischl G, Ziegler S, Kumar P, Wester HJ, Beck R, McEwan AJB, Wiebe LI, Schwaiger M. Hypoxia-specific tumor imaging with F-18-fluoroazomycin arabinoside. Journal of Nuclear Medicine 2005;46:106–113. [PubMed: 15632040]

155. Zhang Y, Chu TW, Gao XG, Liu XQ, Yang Z, Guo ZQ, Wang XY. Synthesis and preliminary biological evaluation of the Tc-99m labeled nitrobenzoimidazole and nitrotriazole as tumor hypoxia markers. Bioorganic & Medicinal Chemistry Letters 2006;16:1831–1833. [PubMed: 16460938]

156. Ballinger JR, Kee JWM, Rauth AM. In vitro and in vivo evaluation of a technetium-99m-labeled 2-nitroimidazole (BMS181321) as a marker of tumor hypoxia. Journal of Nuclear Medicine 1996;37:1023–1031. [PubMed: 8683295]

157. Iyer RV, Haynes PT, Schneider RF, Movsas B, Chapman JD. Marking Hypoxia in Rat Prostate Carcinomas with {beta}-D-[125I]Azomycin Galactopyranoside and [99mTc]HL-91: Correlation with Microelectrode Measurements. J Nucl Med 2001;42:337–344. [PubMed: 11216534]

158. Siim BG, Laux WT, Rutland MD, Palmer BN, Wilson WR. Scintigraphic Imaging of the Hypoxia Marker 99mTechnetium-labeled 2,2′-(1,4-Diaminobutane)bis(2-methyl-3-butanone) Dioxime (99mTc-labeled HL-91; Prognox): Noninvasive Detection of Tumor Response to the Antivascular Agent 5,6-Dimethylxanthenone-4-acetic Acid. Cancer Res 2000;60:4582–4588. [PubMed: 10969810]

159. Cook GJR, Houston S, Barrington SF, Fogelman I. Technetium-99m-Labeled HL91 to Identify Tumor Hypoxia: Correlation with Fluorine-18-FDG. J Nucl Med 1998;39:99–103. [PubMed: 9443745]

160. Schneider RF, Engelhardt EL, Stobbe CC, Fenning MC, Chapman JD. The synthesis and radiolabelling of novel markers of tissue hypoxia of the iodinated azomycin nucleoside class. Journal of Labelled Compounds and Radiopharmaceuticals 1997;39:541–557.

161. Moore R, Chapman J, Mercer J, Mannan R, McEwan A, McPhee M. Measurement of PDT-induced hypoxia in Dunning prostate tumors by I-123-iodoazomycin arabinoside. J Nucl Med 1993;34:405–413. [PubMed: 8441030]

162. Zanzonico P, O'Donoghue J, Chapman JD, Schneider R, Cai S, Larson SD, Wen BX, Chen YC, Finn R, Ruan ST, Gerweck L, Humm J, Ling C. Iodine-124-labeled iodo-azomycin-galactoside imaging of tumor hypoxia in mice with serial microPET scanning. European Journal of Nuclear Medicine and Molecular Imaging 2004;31:117–128. [PubMed: 14523586]

163. Riedl CC, Brader P, Zanzonico PB, Chun YS, Woo Y, Singh P, Carlin S, Wen B, Ling CC, Hricak H, Fong Y. Imaging Hypoxia in Orthotopic Rat Liver Tumors with Iodine 124-labeled Iodoazomycin Galactopyranoside PET1. Radiology 2008;248:561–570. [PubMed: 18641253]

164. Li XF, Sun XR, Ma YY, Suehiro M, Zhang MT, Russell J, Humm JL, Ling CC, O'Donoghue JA. Detection of hypoxia in microscopic tumors using I-131-labeled iodo-azomycin galactopyranoside (I-131-IAZGP) digital autoradiography. European Journal of Nuclear Medicine and Molecular Imaging 37:339–348. [PubMed: 19921184]

165. Fujibayashi Y, Taniuchi H, Yonekura Y, Ohtani H, Konishi J, Yokoyama A. Copper-62-ATSM: A new hypoxia imaging agent with high membrane permeability and low redox potential. Journal of Nuclear Medicine 1997;38:1155–1160. [PubMed: 9225812]

166. Lohith TG, Kudo T, Demura Y, Umeda Y, Kiyono Y, Fujibayashi Y, Okazawa H. Pathophysiologic Correlation Between Cu-62-ATSM and F-18-FDG in Lung Cancer. Journal of Nuclear Medicine 2009;50:1948–1953. [PubMed: 19910425]

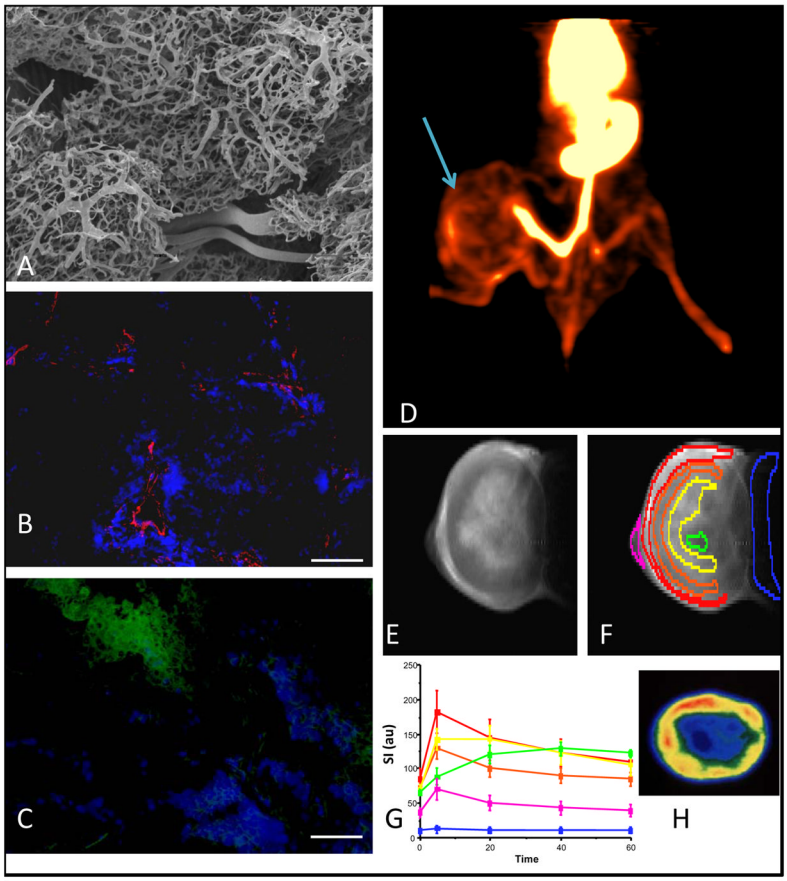

Figure 1. Tumor vascular heterogeneity and hypoxia

Panels each provide evidence for vascular heterogeneity based on *in vivo* and *ex vivo* imaging:

A) Mammary adenocarcinoma 13762NF tumors were grown using a kidney tissue-isolated preparation in adult female Fischer 344 rats. Perfusion of the abdominal aorta proximal to the renal artery with Batson's #17 polymer provided an *ex vivo* 3D representation by means of corrosion casting. Vascular casts were sputtered with gold-palladium prior to Scanning Electron Microscopy. Disorganized vasculature is apparent with many tortuous microvessels and blind ends (data obtained in collaboration with Andrew Abbott and Dr. C. Gilpin).

B) Immunohistochemistry from similar 13762NF tumor. Pimonidazole was infused and 60 mins later Hoechst 33342 dye (seen in blue) was infused IV with tumor excision 60 s later. Frozen 6 μm-thick sections were stained using anti-CD31 mAb (red). Extravasated Hoechst dye surrounded the red blood vessels. Scale bar 100 μm, original magnification x100.

C) Separate section of the same tumor as B. Perfusion is shown by Hoechst dye (blue) and hypoxia in green.

D) Image slice from 3D PET of 13762NF tumor bearing rat 24 hrs after infusion of 41 μCi ^{74}As-SATA-labeled bavituximab - a humanized monoclonal antibody targeting exposed phosphatidylserine of the outer leaflet of stressed vasculature. The tumor (arrow) shows distinct vascular heterogeneity. At this stage, much of the activity was likely still circulating in the vasculature.

E) ^{1}H MRI of slice of Dunning prostate R3327-AT1 tumor obtained 20 mins after IV infusion of Gd-DTPA contrast agent (Magnevist).

F) Same as E with selected regions of interest

G) Time course of signal intensity variations (contrast) in tumor regions delineated in F, showing distinct heterogeneity of perfusion (data obtained in collaboration with Dr. P. Antich).

H) Autoradiography of slice of excised AT1 tumor following infusion of the vascular volume marker ^{125}I-labeled albumin, revealing similar heterogeneity to that detect by MRI in vivo in E-G (data obtained in collaboration with Dr. J Anderson).

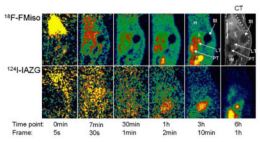

Figure 2. Comparison of F-MISO and 124-IAZAG in rat liver tumors by PET

Images show various time points after the administration on consecutive days of ^{18}F-FMISO (2 mCi; upper row) or ^{124}I-IAZG (1 mCi; lower row) to a rat with Morris hepatoma McA-R-7777. ^{18}F-FMISO localized to the same tumor regions as ^{124}I-IAZG. The contrast ratios (tumor/background) reached similar values for the two hypoxia tracers, but at later times for ^{124}I-IAZG than for ^{18}F-FMISO and, hence poorer count statistics so that the ^{18}F-FMISO images were of superior diagnostic image quality to the ^{124}I-IAZG images. H=heart; L=liver; St=stomach; LT=liver tumor; PT=peritoneal tumor. Reprinted by permission of (44)

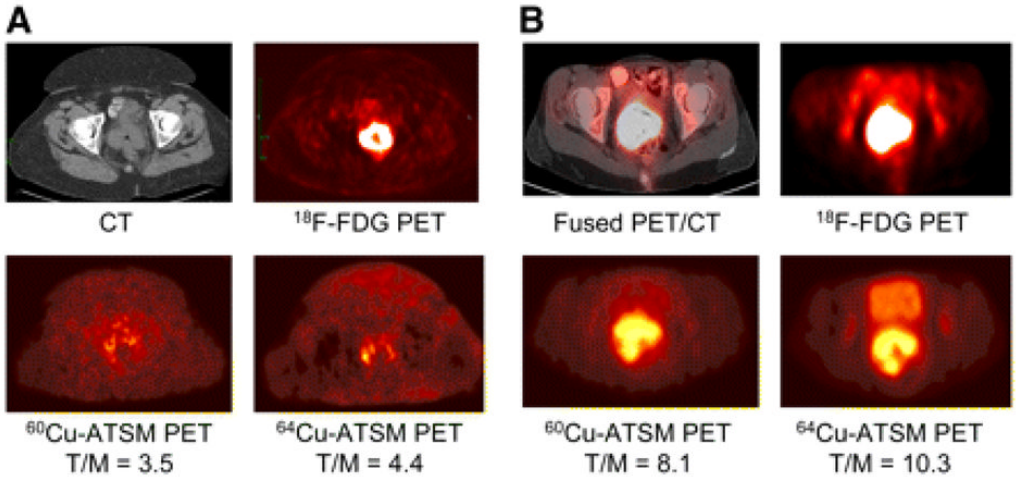

Figure 3. Comparison of ^{60}Cu-ATSM and ^{64}Cu-ATSM in patients with cervical carcinoma using PET

(A) Transaxial CT (top left) and ^{18}F-FDG PET (top right) images of pelvis showing intense ^{18}F-FDG uptake within known cervical tumor seen on CT. Transaxial 30- to 60-min summed images of ^{60}Cu-ATSM PET (bottom left) and ^{64}Cu-ATSM PET (bottom right) of pelvis at same level demonstrate mildly increased uptake within known primary cervical tumor.

(B) Transaxial coregistered ^{18}F-FDG PET/CT (top left) and ^{18}F-FDG PET (top right) images of pelvis show intense ^{18}F-FDG uptake within cervical tumor. Transaxial 30- to 60-min summed images of ^{60}Cu-ATSM PET (bottom left) and ^{64}Cu-ATSM PET (bottom right) of pelvis at same level. Both patients showed similar patterns of ^{60}Cu-ATSM and ^{64}Cu-ATSM uptake within the tumor, though patient (B) showed markedly grater uptake of both agents. The images with ^{64}Cu-ATSM had a slightly better target-to background ratio and tumors were delineated more clearly. Reprinted by permission of the Society of Nuclear Medicine from: Lewis JS, Laforest R, Dehdashti F, et al. An Imaging Comparison of 64Cu-ATSM and 60Cu-ATSM in Cancer of the Uterine Cervix. J Nucl Med. 2008; 49(7): 1177–1182. Figure 3 (48)

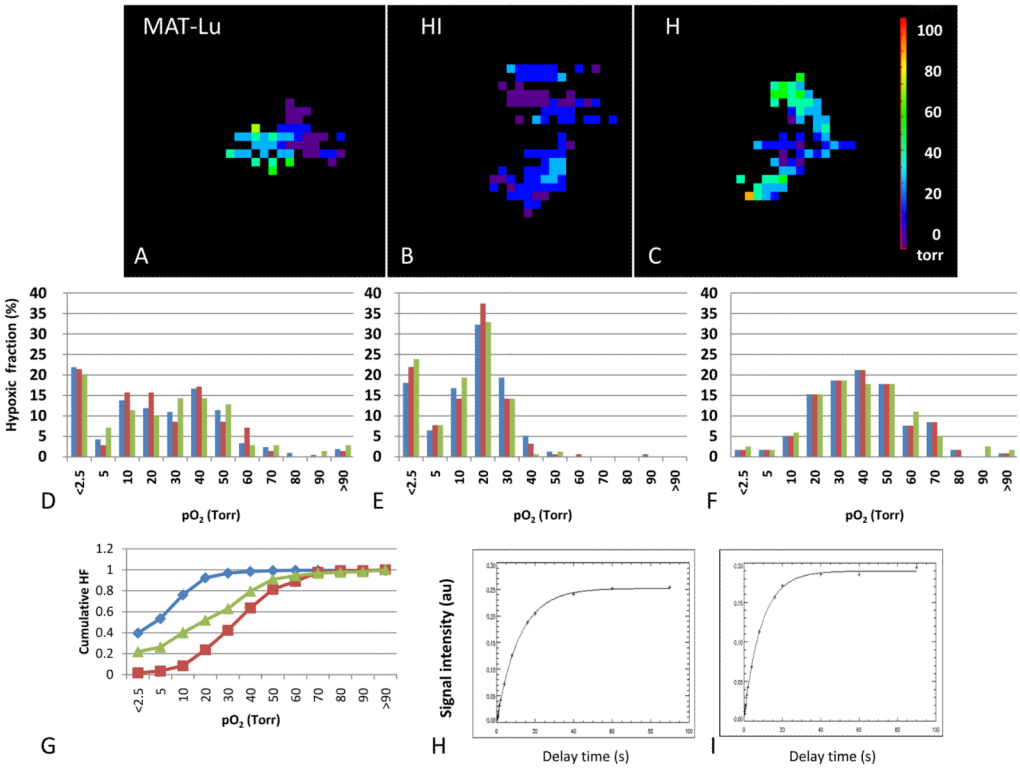

Figure 4. Heterogeneity of tumor oxygenation

Maps of pO_2 were generated using FREDOM following direct injection of 100 μl hexafluorobenzene into the respective Dunning R3327 prostate tumors growing syngeneically on thigh of Copenhagen rats. Each tumor shows a range of pO_2s, which are presented as histograms below. Sequential pO_2 maps were acquired over 20 mins, while anesthetized rats breathed air +1% isoflurane and the baseline stability is revealed by the consistent histograms. For the fast growing small MAT-Lu tumor (**A, D**: volume 1.2 cm^3; volume doubling time ~2 days) mean pO_2=22.1 torr, median pO_2= 19.8 torr and HF_{10}= 40%. For the moderately well differentiated large HI tumor (**B, E**: volume 7.6 cm^3; volume doubling time ~10 days) mean pO_2= 13.4 torr, median pO_2= 13.4 torr and HF_{10}= 76%. For the slow growing small H tumor (**C, F**: volume 0.6; volume doubling time ~20 days) mean pO_2= 36.9 torr, median pO_2= 37.5 torr and HF_{10}= 8%. **G** shows the cumulative hypoxic fraction of each of the tumors MAT-Lu (green); HI (blue) and H (red). These data are quite consistent with the population mean values reported in Table 3. Relaxation curves for representative voxels **H** T_1=11.61 s (pO_2=0.78 torr) and **I** T_1=1.47 s (pO_2=46.5 torr).

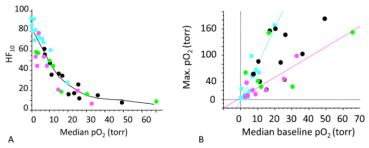

Figure 5. Tumor oxygenation assessed by ^{19}F MRI

A) Relationships between median pO_2 in Dunning prostate R3327 pedicle tumors and hypoxia faction. MAT-Lu (pink); AT1 (blue); HI (green); H (black). As expected a generally inverse relationship was observed based on FREDOM.

B) Baseline pO_2 was measured during air breathing and is related to maximum median pO_2 observed during a hyperoxic gas breathing challenge with oxygen. For any given tumor type a reasonable correlation was found, *e.g.*, pink and blue lines, but each tumor type behaved very differently.

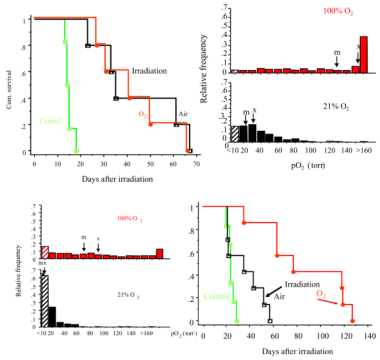

Figure 6. Modulating tumor response to irradiation in Dunning prostate R3327-HI tumors

The Kaplan Meier hazard plots indicate time to reach 2 x initial size (T_2).

Bottom: Large HI tumors exhibit extensive hypoxia (histogram, bottom left), however it is essentially eliminated by breathing oxygen (histogram, top left) resulting in excellent response to irradiation. Here a single dose of 30 Gy (half-the TCD_{50}) was applied and the time to double in size was observed. Tumors on rats breathing air during irradiation showed little benefit over controls. By contrast, a significant growth delay (51 days; $p < 0.01$) was observed in large HI tumors, when rats breathed oxygen 30 min prior to and during irradiation. Baseline hypoxic fraction was high HF_{10}>65%. However, breathing oxygen essentiality eliminated the hypoxic fraction (HF_{10}<20%) and these tumors showed a significant growth delay compared with controls or irradiated air breathing animals.

Top: Small HI tumors, which are well oxygenated, respond to irradiation. Here, a single dose of 30 Gy (half-the TCD_{50}) was applied and the time to double in size was observed. Tumors on rats breathing air (black line) or oxygen (red line) showed a significant growth delay compared with controls (green line). Baseline hypoxic fraction was small HF_{10}<25%. Modified from (85).

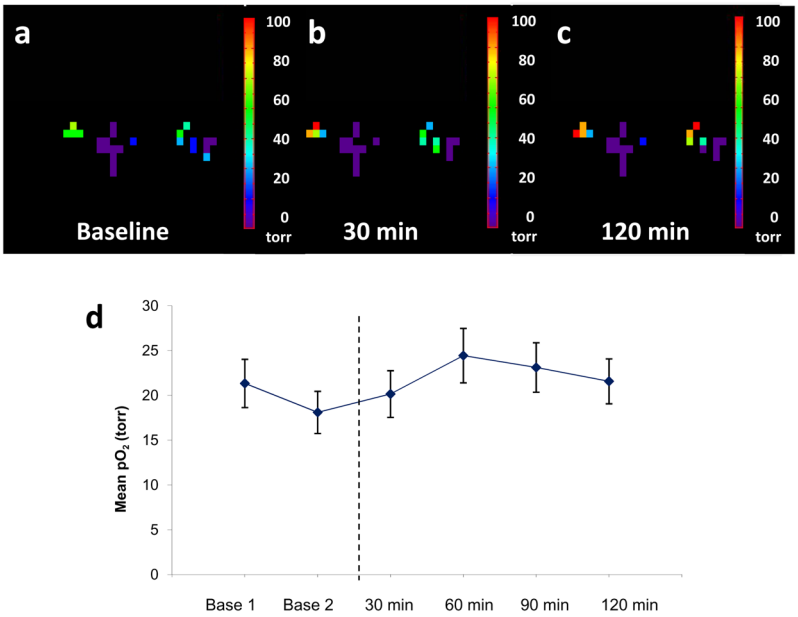

Figure 7. Tumor oxygenation with respect to vascular targeting agent bavituximab

Hexafluorobenzene (50 μl) was injected directly into a small Dunning prostate R3327-AT1 tumor (0.94 cm^3) and pO_2 maps were obtained using FREDOM in 6.5 mins each. Following **a**) baseline measurement, bavituximab was injected (0.35 ml intravenously) and further pO_2 maps were acquired over the following 2 hrs (**b** after 30 mins and **c** after 120 min). **d**) Mean pO_2 values + standard deviation are plotted (d) showing little acute response.

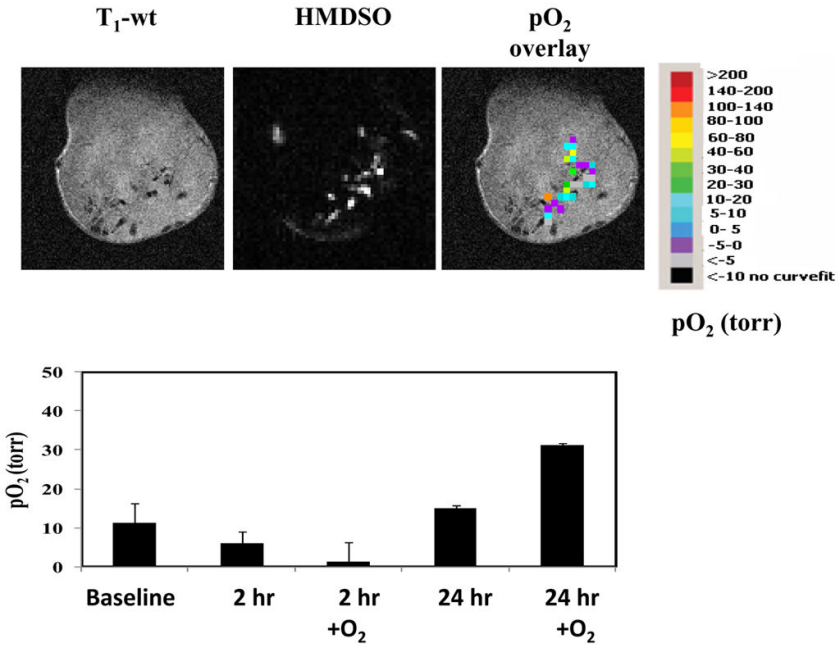

Figure 8. Monitoring oxygenation changes with respect to vascular targeting agent Combretastatin A4-phosphate using PISTOL

HMDSO (100 μl) was injected directly into Dunning R3327-H prostate tumor implanted in a Copenhagen rat. Sequential pO_2 maps were measured before and for 24 hrs following the administration of the vascular disrupting agent Combretastatin A4-phosphate (CA4P; 30 mg/kg). Upper panel shows images on day 1, while the lower panel shows pO_2 dynamics and response to oxygen breathing at 2 and 24 hrs post administration of CA4P compared to baseline (CA4P kindly provided by OxiGene).

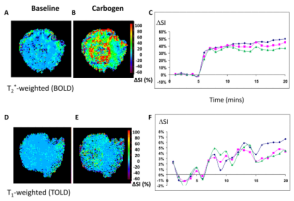

Figure 9. DOCENT

Sequential interleaved T_2*-weighted (BOLD) and T_1-weighted (TOLD) 1H MR images were obtained from HI tumor (0.45 cm^3) during baseline air breathing (**a** BOLD and **d** TOLD, respectively) and with respect to carbogen challenge (**b** and **e** for BOLD and TOLD respectively). **c**) within 2 minutes there was a large significant BOLD response reaching a plateau of about 40% signal enhancement indicating reduced levels of vascular deoxyhemoglobin. **f**) a more sluggish TOLD response was seen over several minutes consistent with delivery of oxygen to the tissues and elevated pO_2. Heterogeneity of signal response was seen within the tumor slice, but three adjacent slices showed remarkably consistent response (green, red and blue lines show mean response for each slice).

Table 1

Tumor Oximetry methods

Technique	Reporter	Parameter	Characteristics	References
Magnetic resonance				
BOLD	Magnetic fields created by deoxyHb Vascular water	R_2*; ΔR_2*ΔSI (T_2*w)	Imaging at high spatial and temporal resolution. Non- invasive. Endogenous contrast with hyperoxic gas challenge. Potential interference from blood flow, volume.	(92,96,100,102,127)
TOLD	Magnetic fields created by O_2 Tissue water	R_1; $\Delta R_1\Delta$SI (T_1w)	Endogenous contrast or hyperoxic gas challenge.	(109,111,128)
^{19}F MR, e.g., FREDOM	HFB	R_1	Map multiple locations each 8 mm^3, 6.5 mins (recently 90 s), direct injection of reporter into tissue using 32G needle	(6,82,89,100,117)
^{19}F MRI	PFC emulsion	R_1, R_2	IV, may bias measurements to perfused regions	(76,77,129,130)
PISTOL	HMDSO	R_1	Map multiple locations in 4.5 mins for pO_2 map- procedure analogous to FREDOM	(91)
DCE MRI	Gd-DTPA	Contrast kinetics	IV, Maps, mins -parameters have been related to pO_2	(131–133)
^{19}F NMR	F-nitroimidazoles	Signal intensity	Hypoxia, not pO_2	(38,39,125)
ESR/EPR	Chars; Phthalocyanine Nitroxides	Linewidth	Needle 23 G IT, single location or maps. Problem of reporter decay	(64,65,69)
Optical				
Phosphorescence	Pd-complex	Lifetime	Vascular signal limited by tissue light penetration	(134)
NIR	Oxy and deoxy hemoglobin	Relative absorption	Vascular signal	(68,82,135)
FLI and BLI with reporter genes under HRE control	eGFP, Luciferase	Signal intensity	Limited tissue light penetration BLI requires luciferin substrate	(19)
Nuclear				
PET	^{18}F misonidazole labeled with ^{18}F 18F EF5 Cu-ATSM (^{60,62,64,} ^{67}Cu)	Tumor to muscle ratio	Non invasive. High sensitivity. Only viable hypoxic cells give signal; radioactive compounds. short half life; small range of pO_2 values covered; low spatial resolution. Cu-ATSM uptake perturbed by MDR transporters.	(17,34,46,47)

Table 2

Radionuclide approaches to assessing tumor hypoxia

			references	
Agent	**nuclide**	**Chemistry for synthesis**	**Pre-clinical applications**	**Clinical applications**
F-MISO (^{18}F-fluoromisonidazole)	^{18}F	(136)	(43,137)	(138)
EF1 (2-(2-Nitroimidazol-1*H*-yl)-*N*-(3-[^{18}F]fluoropropyl)acetamide)	^{18}F	(139)	(140)	none
EF3 (2-(2-nitroimidazol-1-yl)-N-(3[F-18], 3,3-trifluoropropyl) acetamide)	^{18}F	(141)	(142)	(143)
EF5 (2(2-nitro-1H-imidazol-1-yl)-N-(2,2,3,3,3- pentafluoropropyl)acetamide)	^{18}F	(144)	(145,146)	(147)
FETA (fluoroetanidazole)	^{18}F	(148)	(149)	none
FETNIM (Fluorine-18 fluoroerythronitroimidazole)	^{18}F	(150)	(151)	(152)
FAZA (fluoroazomycin arabinoside)	^{18}F	(153)	(43,154)	none
BMS181321 and other ^{99m}Tc-labeled nitroimidazoles HL-91 (PROGNOX)	^{99m}Tc	(155)	(156) (157,158)	(159)
IAZG (iodo-azomycin galactopyranoside)	^{123}I SPECT ^{124}I PET ^{125}I SPECT ^{131}I for therapy + autoradiography	(160)	(161) (43,44,162,163) (157) (164)	NCT00588276 http://clinicaltrials.gov/ct2/show/NCT00588276
Cu-ATSM (diacetyl-bis(N4- methylthiosemicarbazone))	^{60}Cu PET ^{62}Cu ^{64}Cu PET	(165) (45)	(46,47)	(34,48) (166) (48)

Further information on many of these agents is available from the NIH MICAD data base http://www.ncbi.nlm.nih.gov/bookshelf/br.fcgi?book=micad

Table 3

CHARACTERISTICS OF TUMOR SUBLINES

Tumor Dunning prostate R3327 lines	VDT (volume doubling time; days)	Hypoxic fraction HF_{10} (%)		Mean pO_2 (torr)		Response to oxygen breathing
		Small	Large	Small	Large	
MAT-Lu* (84)	2.7	23 14	58 40	24 60	8 27	Slow
AT1 air O_2 (81)	5	61 24	83 59	10 62	4 40	Slow
HI (84,85)	9	20 15*	80 20	29 75*	2 102	Rapid
H air O_2 (81)	16	16 3	46 10	34 137	13 83	Moderate

Small tumors <2 cm^3; large >3.5 cm^3. AT1, HI, and H tumors on rats breathing isoflurane/air;

*older anesthesia protocol using methoxyflurane with 33% O_2/66%N_2O for baseline.